DESIGN AND CONSTRUCTION OF UNMANNED UNDERWATER VEHICLE

A THESIS SUBMITTED TO
THE GRADUATE SCHOOL OF NATURAL AND APPLIED SCIENCES
OF
MIDDLE EAST TECHNICAL UNIVERSITY

BY

FATİH ERCİS

IN PARTIAL FULFILLMENT OF THE REQUIREMENTS
FOR
THE DEGREE OF MASTER OF SCIENCE
IN
MECHANICAL ENGINEERING

JUNE 2013

Approval of the thesis:

DESIGN AND CONSTRUCTION OF UNMANNED UNDERWATER VEHICLE

submitted by **FATİH ERCİS** in partial fulfillment of the requirements for the degree of **Master of Science in Mechanical Engineering Department, Middle East Technical University** by,

Prof. Dr. Canan Özgen
Dean, Graduate School of **Natural and Applied Sciences** _____

Prof. Dr. Süha Oral
Head of Department, **Mechanical Engineering** _____

Prof. Dr. Kemal İder
Supervisor, **Mechanical Engineering Department, METU** _____

Prof. Dr. Haluk Aksel
Co-Supervisor, **Mechanical Engineering Department, METU** _____

Examining Committee Members:

Prof. Dr. Kahraman Albayrak
Mechanical Engineering Dept., METU _____

Prof. Dr. Kemal İder
Mechanical Engineering Dept., METU _____

Prof. Dr. Haluk Aksel
Mechanical Engineering Dept., METU _____

Prof. Dr. Haluk Darendeliler
Mechanical Engineering Dept., METU _____

Prof. Dr. Tolga Çiloğlu
Electrical and Electronics Engineering Dept., METU _____

Date: 25 June 2013

I hereby declare that all information in this document has been obtained and presented in accordance with academic rules and ethical conduct. I also declare that, as required by these rules and conduct, I have fully cited and referenced all material and results that are not original to this work.

Name, Last name : FATİH ERCİS

Signature :

ABSTRACT

DESIGN AND CONSTRUCTION OF UNMANNED UNDERWATER VEHICLE

Ercis, Fatih
M.Sc., Department of Mechanical Engineering
Supervisor: Prof. Dr. Kemal İder
Co-Supervisor: Prof. Dr. Haluk Aksel

June 2013, 62 pages

In this thesis, one type of unmanned underwater vehicle (UUV) is designed and constructed. The vehicle is used as target emulator in defence industry. The target emulator consists of five subsystems. They are hull, thrust system, anti-roll fins and eccentric weight, stability fins and control fin system. The hull has hydrodynamic outer geometry so that the UUV reaches to the required speed. The thrust system consists of propeller, propeller shaft, bearings, coupling and servo motor. Some sealing elements and are used to protect the hull against water at the maximum working depth. The propeller of target emulator creates both thrust and roll moment. To control target emulator, the roll moment must be eliminated. Therefore, two methods which are anti-roll fins and eccentric weight are used together to do. The stability of the device is also important during and after the launch. To improve the stability, stability fins are designed and one of them is selected according to the launch tests. Besides, speed tests are performed to measure the speed of the target emulator and the roll angle. Two alternative control fin systems are designed to control the vehicle. Both of them are manufactured and they are compared with regards to efficiency, precision, complexity and cost. In conclusion, finite element analysis of hull is carried out to find the equivalent stresses and strains of hull.

Keywords: Unmanned Underwater Vehicle, Design and Construction, Finite Element Analysis

ÖZ

İNSANSIZ DENİZALTI ARACININ TASARIMI VE KONSTRÜKSİYONU

Ercis, Fatih
Yüksek Lisans, Makina Mühendisliği Bölümü
Tez Yöneticisi: Prof. Dr. Kemal İder
Ortak Tez Yôneticisi: Prof. Dr. Haluk Aksel

Haziran 2013, 62 sayfa

Bu tezde bir insansız denizaltı aracının (İDA) tasarımı ve konstrüksiyonu yapılmıştır. Bu araç aldatıcı olarak savunma endüstrisinde kullanılmaktadır. Aldatıcı beş alt sistemden oluşmaktadır. Bu beş alt sistem dış gövde, itki sistemi, anti-yuvarlanma ve eksantrik ağırlık, stabilite kanatçıkları ve kontrol kanatçık sistemleridir. İDA'nın istenen hıza ulaşması için dış gövde geometrisinin hidrodinamik bir yapıda olması gerekmektedir. İtki sistemi pervane, pervane mili, rulmanlar, kaplin ve servo motordan oluşmaktadır. Bazı sızdırmazlık elemanları gövdenin maksimum çalışma derinliğinde sudan korunması için kullanılmıştır. Pervane hem itki hem de dönme momenti yaratmaktadır. Aldatıcıyı kontrol etmek için dönme momenti etkisiz hale getirilmelidir. Dolayısıyla bunu sağlamak için anti-yuvarlanma kanatçıkları ve eksantrik ağırlık metotları birlikte kullanılmıştır. Ayrıca bu cihazın atış esansında ve sonrasında stabilitesi önemlidir. Stabiliteyi artırmak için stabilite kanatçıkları tasarlanmış ve bunlardan biri atış testlerine göre seçilmiştir. Ayrıca hız testleri yapılarak aldatıcının hızı ve dönme açısı ölçülmüştür. Bu aracı kontrol etmek için iki alternatif kontrol kanatçık sistemi tasarlanmıştır. İki tasarım da üretilmiş ve verimlilik, hassasiyet, karmaşıklık ve maliyet açısından karşılaştırılmışlardır. Son olarak, sonlu elemanlar analizi yapılarak gövdenin eşdeğer stresleri ve gerinimleri bulunmuştur.

Anahtar Kelimeler: İnsansız Denizaltı Aracı, Tasarım ve Konstrüksiyon, Sonlu Elemanlar Analizi

To all members of my family

ACKNOWLEDGMENTS

I express sincere appreciation to Prof. Dr. Kemal İder and Prof. Dr Haluk Aksel for their guidance, advice, criticism, systematic supervision, encouragements, and insight throughout the study.

The author would also like to thank Prof. Dr. Tolga Çiloğlu for his suggestions and comments.

I wish to thank Mr. Necati Karaismailoğlu, Mr. Diren Abat from ASELSAN. The technical assistance of them is gratefully acknowledged.

Special thanks go to my colleagues, Kadir Ali Gürsoy, Ali Karakuş, Alp Emre Öngüt, Ali Murat Kayıran.

I also want to thank my beloved family, Mehmet Özkan Ercis, Nimet Ercis, Yavuz Selim Ercis and my dearest friends, Özge Büşra Hacı, Ertuğrul Özcan, Gökhan Oktay, Fırat Gürsey for their encouragement and faith in me.

TABLE OF CONTENTS

LIST OF TABLES

TABLES

LIST OF FIGURES

FIGURES

CHAPTER 1

INTRODUCTION

Up to recently, unmanned underwater vehicles (UUV) have been used for a limited number of applications in industry. With advancing technology, the unmanned underwater vehicles find themselves more and more application areas. In this thesis, one type of unmanned underwater vehicle is designed and constructed. The type is target emulator and it has propeller. The target emulator has also control fins which are used to move it. The vehicle is used as a countermeasure decoy to protect submarines and ships from the attack of threats of enemy torpedoes. In introduction chapter will be mentioned literature survey about anti-torpedo countermeasures and working principles of the vehicles. Then, the chapter continues with the general design requirements and range of the thesis.

1.1 Target Emulators

Capabilities of torpedoes are continuously improved. To measure their serious threats on military or any vehicles, some devices must be developed. Thus, the devices are developed to satisfy that requirement. However, there is little real progress in the development of anti-torpedo measures since the Second World War for both submarines and surface ships. For both, the current primary method of defence remains a towed or expendable noisemaker, with the bubble generator, which uses a chemical reaction to produce a large cloud of bubbles to act as a false target, remaining a primary countermeasure for submarines. Not until the late 1980s was any real progress made in the field of acoustic countermeasures.

Our device uses the method of acoustic countermeasure. The device is called as target emulator. It simulates the surface vessel or submarine to protect from torpedoes for a while. Thanks to that, the surface ship or submarines save time to escape. Thus, the system is very important to defence them.

1.2 Literature Survey about Target Emulator

The acoustic countermeasures are devices having new technology. Thus, only limited countries can develop those devices. So, literature survey covers few examples of target emulators.

1.2.1 LESCUT Anti Torpedo Countermeasure

LESCUT is product of the Israeli Company Rafael Advanced Defence Systems Ltd. It is designed to identify the incoming threat and provide a customized response. Surface vessel launched, LESCUT is designed to respond simultaneously to multiple torpedoes of various types active, passive, and Pactiv and programmed to defeat all types of modern torpedo logic. LESCUT operates for ten minutes, then self-destructs and sinks [1].

Table 1.1: Technical Specifications of LESCUT [1].

LESCUT	
Diameter (mm)	123.75
Length (mm)	914-1227
Weight (kg)	4.5- 24.8

Figure 1.1: LESCUT Anti Torpedo Countermeasure [1]

1.2.2 SCUTTER Anti Torpedo Countermeasure

SCUTTER is produced by the Israeli Company Rafael Advanced Defence Systems Ltd. It has developed self-propelled, reactive, expendable torpedo decoy capable of protecting a submarine from acoustic homing, active and/or passive torpedoes. SCUTTER is currently operational in several advanced navies. It provides complete 360° protection of the submarine. SCUTTER can be launched through standard signal ejectors or external launchers and 4" submarine signal ejector (SSE) [2].

Table 1.2: Technical Specifications of SCUTTER [2]

SCUTTER	
Diameter (mm)	101
Length (mm)	1020
Weight (kg)	7.8
Operating Depth (m)	10-300

Figure 1.2: SCUTTER Anti Torpedo Countermeasure [2]

1.2.3 C310 and C303/S Anti Torpedo Countermeasure

C310 and C303/S is produced by WASS which is Finmeccanica Company. They are an anti-torpedo countermeasure systems for surface ships and submarines, designed to cope with current and future generation of active and/or passive torpedoes, wire or non-wire-guided, launched alone or in salvo mode. The system includes mobile target emulators and a launching system. C310 is used to surface ships, whereas C303/S is for submarines [3, 4].

Table 1.3: Technical Specifications of C310 [3]

C310	
Diameter (mm)	127
Length (mm)	1150
Weight (kg)	16

Table 1.4: Technical Specifications of C310 Mobile Target Emulator [3]

C310 Mobile Target Emulator	
Diameter (mm)	127
Length (mm)	1150
Weight (kg)	16

Figure 1.3: C310 Anti Torpedo Countermeasure [3]

Figure 1.4: C310 Mobile Target Emulator Anti Torpedo Countermeasure [3]

Table 1.5: Technical Specifications of C303/S [4]

C303/S	
Diameter (mm)	96,2
Length (mm)	1125
Weight (kg)	6

Table 1.6: Technical Specifications of C303/S MTE [4]

C303/S MTE	
Diameter (mm)	127
Length (mm)	1125
Weight (kg)	15

Figure 1.5: C303 Anti Torpedo Countermeasure [4]

1.2.4 SCAD 101/102 Anti Torpedo Countermeasure

SCAD 101 and 102 are manufactured by Ultra Electronics Ocean Systems. They are self-contained externally mounted and launched torpedo countermeasure fitted to UK Vanguard and planned for astute class submarines. The SCAD 101 countermeasure has acoustic multi-mode capability and is completely programmable by the user. Communications with the store including mission programming is available up until the device is launched. Once launched the countermeasure executes its mission and then scuttles to the ocean bottom. Besides, SCAD 102 is currently fitted to all UK submarines [5].

Table 1.7: Technical Specifications of SCAD 101/102 [5]

SCAD 101/102	
Diameter (mm)	100
Length (mm)	1000

Figure 1.6: SCAD 101/102 Anti Torpedo Countermeasure [5]

1.2.5 ISiMI

The Korea Ocean Research and Development Institute (KORDI) has developed a small AUV named ISiMI. The ISiMI system is divided into a mechanical system, a control system. Its mechanical system includes its hull structure, its thruster and its control fins. Its control system includes a computer, electrical interface boards, sensors and software [6].

1.2.5.1 Mechanical System

The hull size of the ISiMI AUV is constrained by the space for the on board instruments, and the hull shape is constrained by the AUV's hydrodynamic characteristics. The standard hull length and diameter are 1.2 and 0.17 m, respectively, considering the installation of the on board equipment. The hull shape of the ISiMI AUV was designed based on the Myring hull profile equations (Myring, 1976), which are known as the best contours for minimizing the drag coefficient for a given ratio of body length and diameter [6].

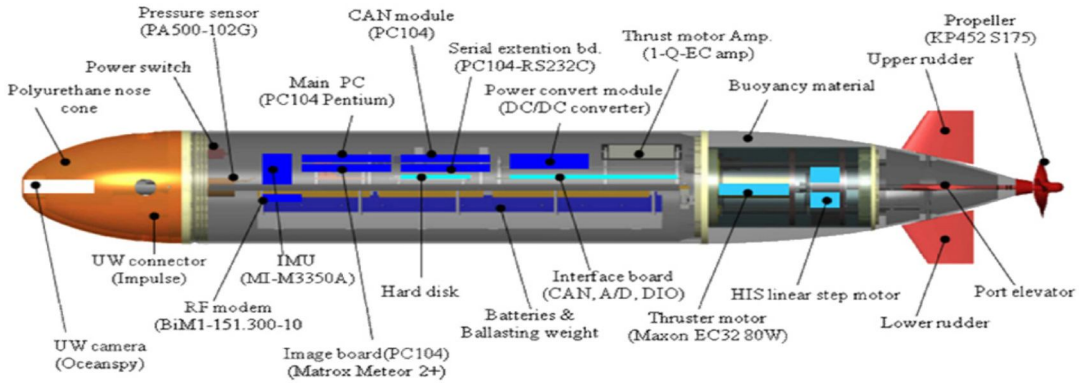

Figure 1.7: General arrangement of the AUV ISiMI system [6]

Table 1.8: Technical Specifications of ISiMI [6]

ISiMI	
Diameter (mm)	170
Length (mm)	1196
Weight (kg)	15
Speed (m/s)	1.0

1.2.5.2 Control System

The NACA 0012 cross-section was adopted for the control plane. Linear stepper motors were chosen for the fin actuators. The pair of rudders is controlled by a linear stepper motor, and the two stern elevators are independently driven by two linear stepper motors. Assuming the maximum torque required by the control fin is 10 kg cm, including the torque margin for mechanical loss, and assuming that the distance between the fin shaft and the driving axis is 5 cm, we chose a 25N stepper motor for each elevator and a 50N motor for the rudders [6].

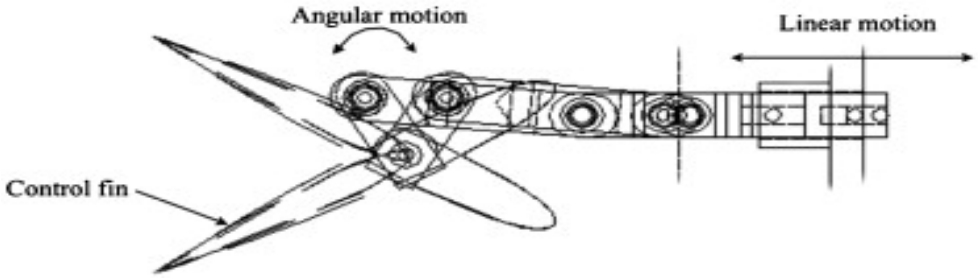

Figure 1.8: Structure of the control fin [7]

1.3 General Mechanical Design Requirements

The final design of target emulator with propeller should

- be able to have minimum 8 minutes operating life,
- have **Confidential** maximum diameter and **Confidential** mm maximum length,
- be able to work at depths between 0-300 meters,
- be able to reach maximum speed of **Confidential**,
- be able to go away enough from the submarine provided that the design is not affected from or it does not affect the submarine and its propeller when decoy is launched,
- be controlled by a control mechanism,
- be stable during its movement

1.4 Subsystems of UUV

1.4.1 Hull

The hull must have hydrodynamic outer geometry so that the UUV reaches to required speed of **Confidential**. Ropeway tests are performed to observe the hydrodynamic performance of the outer geometry. Furthermore, some sealing elements are used to prevent leakage and static leakage tests are carried out to observe whether the body is watertight at different pressures.

1.4.2 Thrust System

A thrust system is designed to move the UUV. The system generally consists of propeller, shaft, propeller shaft, sealing element, shaft bearings and coupling. The shaft sealing element is also tested in leakage tests. Ropeway tests are also carried out whether propeller performance and anti-roll fins are sufficient or not.

1.4.3 Anti-Roll Fins and Eccentric Weight

UUV's propeller creates both thrust force and roll moment. The roll moment prevents controlling the UUV. Thus, the moment must be balanced by another moment. To do that, two methods are used together. They are eccentric weights and anti-roll fins. Besides, anti-roll fins and eccentric weights are tested in ropeway and adjustable ejector tests.

1.4.4 Stability Fins

Two types of stability fins are designed in order that the UUV moves stable during and after launch. The fins are compared by adjustable ejector test setup.

1.4.5 Control Fin System

Control fin system is necessary to move the UUV and two control fins are used to do that. Two alternative control mechanisms are designed to move the control fins. Finally, one of them is selected.

1.5 Aim and Outline of the Thesis

This thesis includes all the mechanical design and construction of target emulator. The brief of the thesis is as following;

In Chapter 2,

The chapter consists of some fundamental dynamic concepts and factors affecting the dynamics of unmanned underwater vehicles (UUV).

In Chapter 3,

In this chapter, the hull is designed and some calculations are made for the hull thickness. The thrust system is explained and its components are designed.

In Chapter 4,

In Chapter 4, the control fin system of UVV is designed and constructed. Two alternative control fin systems are designed and compared. Finally, one of them is selected and manufactured.

In Chapter 5,

Some finite element analyses are performed in this chapter. The results of the analyses are compared with the calculations made in Chapter 3

CHAPTER 2

DYNAMICS OF UUV

This chapter introduces some of fundamental dynamic concepts and factors affecting the dynamics of unmanned underwater vehicles.

2.1 UUV Coordinate System

Unmanned underwater vehicle has 6 DOF. They are three spatial coordinates, x, y and z and three attitude defining Euler angles, roll, pitch and yaw (Figure2.1) [8].

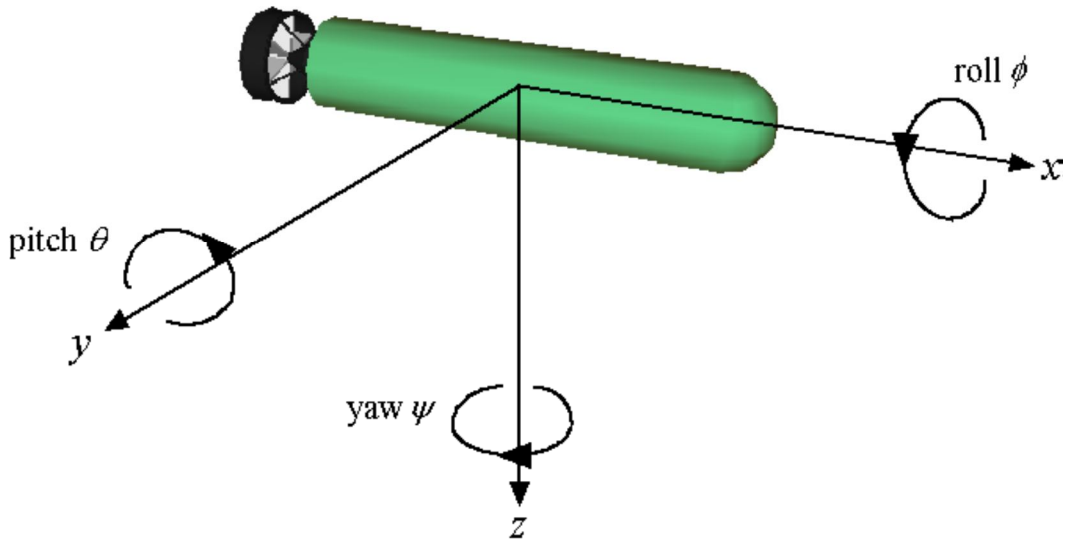

Figure 2.1: Coordinate Axis and 6 DOF of UUV [8]

In this application, we want to control target emulator and therefore roll, pitch and yaw angles and their moments are the important parameters.

2.2 Factors Affecting UUV Dynamics

With regard to UUV dynamics, factors such as buoyancy, hydrodynamic drag and lift, added mass, pressure and environmental forces have to be taken into consideration.

2.2.1 Buoyancy

The magnitude of the buoyant force, B, exerted on a body, floating or submerged, is equal to the weight of the volume of water displaced by that body. The ability of an object to float depends on whether or not the magnitude of the weight of the body, W, is greater than the buoyant force. Clearly, if B > W, then the body will float, while if B < W it will sink. If B and W equate, then the body remains where it is [8].

2.2.2 Hydrodynamic Lift and Drag

When a body is moving through the water, the water creates hydrodynamic lift and forces. These forces have a significant effect on the dynamics of an underwater vehicle which leads to nonlinearity. Therefore, lift and drag forces are taken into account [8].

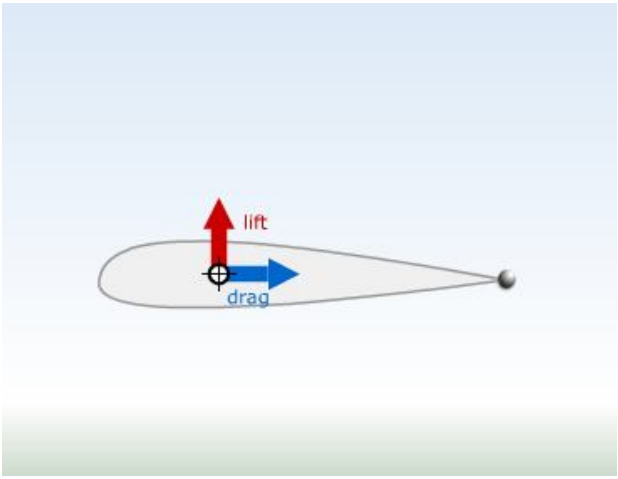

Figure 2.2: Drag and Lift Forces on Hydrodynamic Body

2.2.3 Pressure

As with air, underwater pressure is caused by the weight of the medium, in this case water, acting upon a surface. Pressure is usually measured as an absolute or ambient pressure; absolute denoting the total pressure and ambient being of a relativistic nature. At sea level, pressure due to air is 0.1MPa. For every 10m of depth, pressure increases by about 1atm and hence, the absolute pressure at 10m underwater is 0.2MPa. Although linear in nature, the increase in pressure as depth increases is significant and underwater vehicles must be structurally capable of withstanding a relatively large amount of pressure if they are to survive [8].

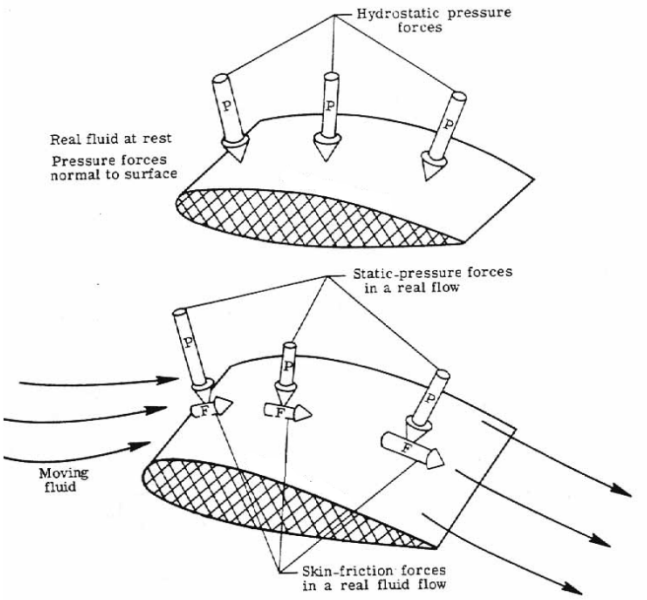

Figure 2.3: Skin Friction and Pressure Forces on Hydrofoil

2.2.4 Added Mass

Another phenomenon that affects underwater vehicles is added mass. When a body moves underwater, the immediate surrounding fluid is accelerated along with the body. This affects the dynamics of the vehicle in such a way that the force required to accelerate the water can be modelled as an added mass. Added mass is a fairly significant effect and is related to the mass and inertial values of the vehicle [8].

2.2.5 Environmental Forces

Environmental disturbances can affect the motion and stability of a vehicle. This is particularly true for an underwater vehicle where waves, currents and even wind can perturb the vehicle. When the vehicle is submerged, the effect of wind and waves can be largely ignored. The most significant disturbances then for underwater vehicles are currents [8].

CHAPTER 3

HULL AND THRUST SYSTEM DESIGN

3.1 Hull Design

The unmanned underwater vehicle is required to have a speed of **Confidential**. Thus, the hull profile of target emulator should have hydrodynamic structure to reach speed of **Confidential** and have also maximum inner volume for placement of other equipment of the decoy. The hydrodynamic outer geometry obtained by the CFD design team of the project is shown in Figure 3.1

Figure 3.1: 200 mm in length conical hull

The fundamental material requirements are machinability, moderate strength, availability and low weight. The material should be stored places where are humidity high. Thus, corrosion properties of the selected material should be adequate. In respect to this, we have selected the material as **Confidential** which is aluminium alloy. **Confidential** has high corrosive resistance, good machinability, moderate strength, low density and the availability of **Confidential** is high [9]. We have used this material for the target emulator casing.

3.2 Predetermination of Thickness and Stress Calculations

We have firstly selected the thickness of hull as 2mm for the calculations. The hull of target emulator must endure mainly two loads. 5MPa pressure is applied to the back side of decoy to launch target emulator and the other load results from hydrostatic pressure.

In calculations, target emulator is fixed to see worst case scenario during the launch. We have also assumed the hull geometry of target emulator as a closed cylinder to simplify the calculations.

3.2.1 Axial Stresses during the Launch

5MPa pressure creates an axial force on the UUV.

$p_{sse} = 5MPa$

That pressure acts on the back side of UUV and it exerts an axial force on the diameter which is 100 mm. It is

$$F_{sse} = A_{\max} p_{sse} \tag{3.1}$$

$F_{sse} = 38.5kN$

We have selected the thickness of decoy as 2mm. Therefore the cross sectional area of decoy, A_c

$$A_c = \frac{\pi(d_o{}^2 - d_i)}{4} = 6.16x10^{-4} \ \ m^2 \tag{3.2}$$

And the axial stress,

$$\sigma_{ax} = \frac{F_{net}}{A_c} = \frac{38.5kN}{6.16x10^{-4}} = 62.5MPa \ \text{(Compression)} \tag{3.3}$$

3.2.2 Hydrostatic Stresses on UUV surface

If we consider the UUV as a capped cylinder, we can use the following equations to find the tangential, longitudinal and radial stresses due to hydrostatic pressure. These cylindrical stresses represent the principal stresses and can be computed directly. Thus we do not need to use Mohr's circle to assess the principal stresses.

Tangential Stress:

$$\sigma_t = \frac{p_i r_i^2 - p_o r_o^2 - r_i^2 r_o^2 (p_o - p_i)/r^2}{r_o^2 - r_i^2} \qquad r_i \le r \le r_o \tag{3.4}$$

Radial Stress:

$$\sigma_r = \frac{p_i r_i^2 - p_o r_o^2 + r_i^2 r_o^2 (p_o - p_i)/r^2}{r_o^2 - r_i^2} \qquad r_i \le r \le r_o \tag{3.5}$$

Longitudinal Stress:

Only valid far away from end caps where bending, nonlinearities and stress concentrations are not significant.

$$\sigma_l = \frac{p_i r_i^2 - p_o r_o^2}{r_o^2 - r_i^2} \qquad r_i \le r \le r_o \tag{3.6}$$

r_i is the inside diameter of cylinder, r_o is the outside diameter, r is anywhere between outside and inside the diameter, p_i is internal pressure and p_o external pressure [10]. If we choose $r = r_o$ to get maximum stresses for tangential stress and $r = r_i$ for radial stress

$$p_o = \rho g h + p_{atm} = (1040 kg/m^3)(300m)(9.81 m^2/s) + (101325 N/m^2) = 3.162 MPa \tag{3.7}$$

$p_i \approx 101325 MPa$

r_i = 0.096 m, r_o = 0.1m

$\sigma_t = -75.12 MPa$, $\sigma_r = -0.1 MPa$, $\sigma_l = -39 MPa$

The stresses are principal stresses. If we combine the axial stresses,

$\sigma_{cl} = -39 - 62.5 = -101.5 MPa$

Finally, we can find equivalent stress by using von Mises stress theory (Distortion energy theory for ductile materials).The theory is

$$\sigma' = \left[\frac{(\sigma_1 - \sigma_2)^2 + (\sigma_2 - \sigma_3)^2 + (\sigma_1 - \sigma_3)^2}{2} \right]^{1/2} \tag{3.8}$$

$$\sigma' = 91.12 \ MPa \tag{3.9}$$

Yielding occurs when

$$\sigma' \geq S_y \tag{3.10}$$

The yield strength of **Confidential** is $S_y = 276MPa$

Thus, the safety factor, n

$$n = \frac{S_y}{\sigma'} = \frac{276}{91.12} = 3.02 \tag{3.11}$$

Nevertheless, if we consider the strength loss of **Confidential** due to corrosion after 10 years of storage at atmospheric exposure, the strength decreases about 5% according to Davis J.R [11] and therefore the safety factor reduces to 2.87. It can be considered that the safety factor is sufficient to design. The calculations are compared with results of the finite element analysis (FEA) in Chapter 5.

3.3 Thrust System

A thrust system is designed to give thrust to the target emulator. The thrust system generally consists of an electric motor, a coupling, a shaft, a propeller and bearings. Many propellers are chosen and tested. One of those is shown in Figure 3.3. The selected motor has adequate torque to rotate the propeller shaft.

Figure 3.2: The Selected Servo Motor

Figure 3.3: The propeller

Coupling is a device used to connect two shafts together at their ends for the purpose of transmitting power. The primary purpose of couplings is to join two pieces of rotating equipment while permitting some degree of misalignment or axial movement or both [12].

There are many types of couplings. An elastic coupling is selected to connect the servo motor and propeller shafts to each other. Elastic couplings can take shock loads and misalignments. Nevertheless, the amount of misalignment is not very large. Installation and maintenance of the elastic couplings are easy.

Figure 3.4: The elastic coupling

3.3.1 Propeller Shaft Design

Propellers create both thrust force and roll moment. The propeller shaft must endure these forces. Tank tests are performed to measure these loads separately.

To measure the thrust force, a test setup is designed. The setup consists of a wood frame, two digital balances and motor-propeller shaft assembly shown in Figure 3.5. The wood frame has a hole through which the propeller shaft can pass. The setup is submerged into a water tank and the thrust force is read by using the balance scale.

Figure 3.5: The tank test setup for measuring thrust force

The roll moment is measured by using a similar test setup. In the roll test setup, an arm connected to the flange of motor-propeller shaft assembly and a balance is used to measure the roll moment. The roll moment is calculated by multiplying the arm length and the amount of reaction force which is read on the balance scale.

Figure 3.6: The tank test setup for measuring roll moment

Graphs illustrating roll moment and thrust force at different motor speeds are shown in the Figure 3.7 and 3.8 corresponding to the propeller shown in Figure 3.3

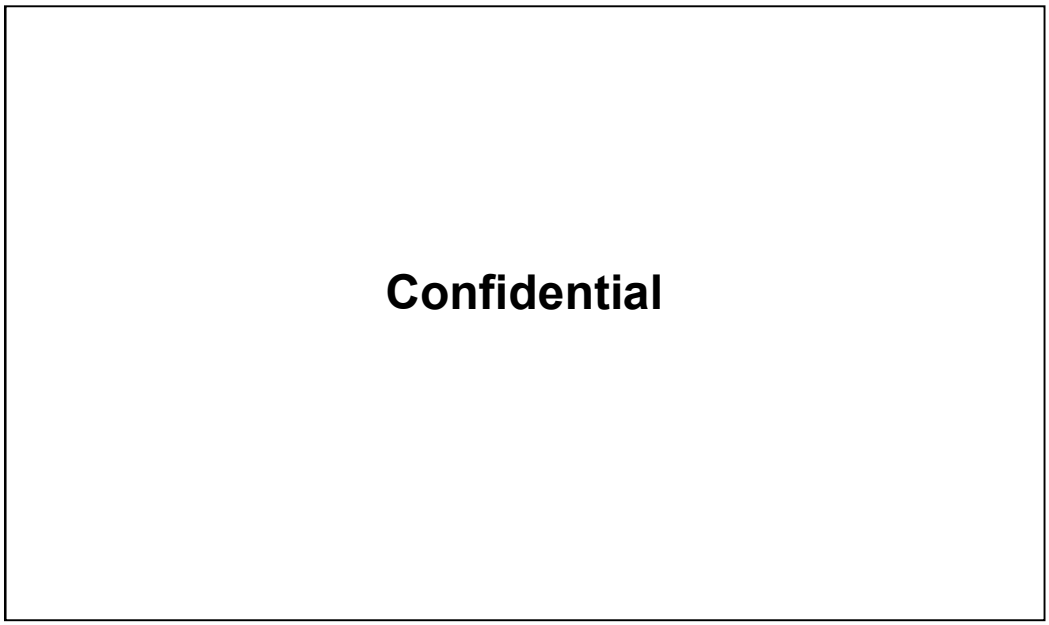

Figure 3.7: The roll moment of propeller at different speeds

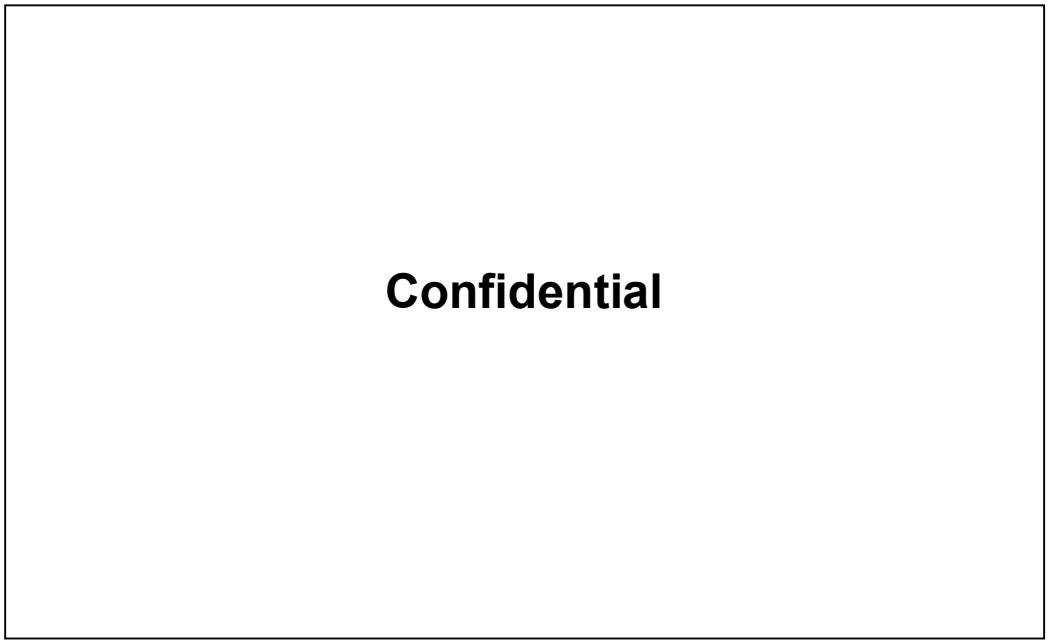

Figure 3.8: The thrust force of propeller at different speeds

According to the CFD design team of the project, the propeller must produce minimum **Confidential** thrust force to reach the UUV speed of **Confidential**. It is inferred that 5000 rpm motor speed is required to obtain **Confidential** thrust force from Figure 3.8. Besides, the roll moment of propeller at 5000 rpm motor speed is about **Confidential**

The shaft of propeller should rotate at this motor speed without failure. The thrust force and roll moment create reaction forces on the shaft. Nevertheless, the stresses created by the reaction forces are low when we compare them with the yield strength of **Confidential** which is $S_y = 276$ MPa

3.3.1.1 Shaft Critical Speed Analysis

Although the propeller shaft is subject to low loads, the shaft may fail due to resonance. Resonance occurs when shaft vibrate at a frequency which close to one of the natural frequencies. Therefore, we have used finite element method to know whether the shaft vibrates at or near resonance frequency.

To obtain the natural frequencies, the shaft body has divided into six finite elements and the six elements have seven nodes.

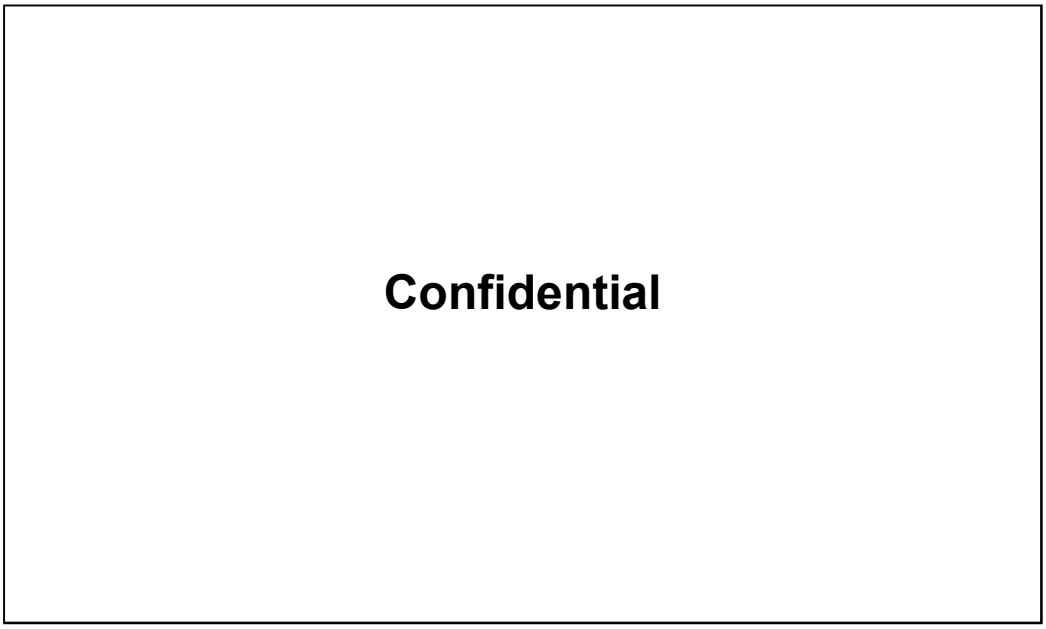

Figure 3.9: The shaft dimensions and finite elements

Depending on the shaft geometry the element length and diameter are different from each other. The element mass and stiffness matrices of the each element are calculated according to following formulas;

$$M^i = \rho AL \begin{bmatrix} \frac{1}{3} & 0 & 0 & \frac{1}{6} & 0 & 0 \\ & \frac{13}{35}+\frac{6}{5}\frac{r^2}{L^2} & \frac{11}{210}L+\frac{1}{10}\frac{r^2}{L} & 0 & \frac{9}{70}-\frac{6}{5}\frac{r^2}{L^2} & -\frac{13}{420}L+\frac{1}{10}\frac{r^2}{L} \\ & & \frac{1}{105}L^2+\frac{2}{15}r^2 & 0 & \frac{13}{420}L+\frac{1}{10}\frac{r^2}{L} & 0 \\ & \text{SYM} & & \frac{1}{3} & 0 & 0 \\ & & & & \frac{13}{35}+\frac{6}{5}\frac{r^2}{L^2} & -\frac{11}{210}L+\frac{1}{10}\frac{r^2}{L} \\ & & & & & \frac{1}{105}L^2+\frac{2}{15}r^2 \end{bmatrix}$$

$$K^i = \begin{bmatrix} \frac{EA}{L} & 0 & 0 & -\frac{EA}{L} & 0 & 0 \\ & \frac{12EI}{L^3} & \frac{6EI}{L^2} & 0 & -\frac{12EI}{L^3} & \frac{6EI}{L^2} \\ & & \frac{4EI}{L} & 0 & -\frac{6EI}{L^2} & \frac{2EI}{L} \\ & & & \frac{EA}{L} & 0 & 0 \\ & \text{SYM} & & & \frac{12EI}{L^3} & -\frac{6EI}{L^2} \\ & & & & & \frac{4EI}{L} \end{bmatrix}$$

Then, we can calculate the global stiffness and mass matrix as following;

$$K = \sum_{i=1}^{6} B^{i^T} K^i B^i \tag{3.15}$$

$$M = \sum_{i=1}^{6} B^{i^T} M^i B^i \tag{3.16}$$

K : Global Stiffness Matrix (21x21)

M : Global Mass Matrix (21x21)

K^i : Element Stiffness Matrix (6x6)

M^i : Element Mass Matrix (6x6)

B^i : Element Boolean Matrix (6x21)

For example, Boolean matrix of first element

$$B^1 = \begin{bmatrix} 1 & 0 & 0 & 0 & 0 & 0 & 0 & 0 & 0 & 0 & 0 & 0 & 0 & 0 & 0 & 0 & 0 & 0 & 0 & 0 & 0 \\ 0 & 1 & 0 & 0 & 0 & 0 & 0 & 0 & 0 & 0 & 0 & 0 & 0 & 0 & 0 & 0 & 0 & 0 & 0 & 0 & 0 \\ 0 & 0 & 1 & 0 & 0 & 0 & 0 & 0 & 0 & 0 & 0 & 0 & 0 & 0 & 0 & 0 & 0 & 0 & 0 & 0 & 0 \\ 0 & 0 & 0 & 1 & 0 & 0 & 0 & 0 & 0 & 0 & 0 & 0 & 0 & 0 & 0 & 0 & 0 & 0 & 0 & 0 & 0 \\ 0 & 0 & 0 & 0 & 1 & 0 & 0 & 0 & 0 & 0 & 0 & 0 & 0 & 0 & 0 & 0 & 0 & 0 & 0 & 0 & 0 \\ 0 & 0 & 0 & 0 & 0 & 1 & 0 & 0 & 0 & 0 & 0 & 0 & 0 & 0 & 0 & 0 & 0 & 0 & 0 & 0 & 0 \end{bmatrix}$$

The system has 21 degree of freedom. However, the shaft is supported by two bearings. The shaft is fixed at the point B and is free axially at the point E so that thermal expansion doesn't create thermal stress on the shaft.

Before boundary conditions are applied, the body nodal variable vector is

$$\alpha = [u_1^A, u_2^A, \theta^A, u_1^B, u_2^B, \theta^B, u_1^C, u_2^C, \theta^C, u_1^D, u_2^D, \theta^D, u_1^E, u_2^E, \theta^E, u_1^F, u_2^F, \theta^F, u_1^G, u_2^G, \theta^G]^T \qquad (3.17)$$

u_1^i = Axial deformation nodal variable

u_2^i = Bending deflection nodal variable

θ^i = Bending rotation nodal variable

The element nodal variable vector;

$$\alpha^i = B^i \alpha \qquad (3.18)$$

α^i : Element nodal variable vector (6x1)

α : Body nodal variable vector (21x1)

$$\alpha^1 = [u_1^A, u_2^A, \theta^A, u_1^B, u_2^B, \theta^B]^T$$
$$\alpha^2 = [u_1^B, u_2^B, \theta^B, u_1^C, u_2^C, \theta^C]^T$$
$$\alpha^3 = [u_1^C, u_2^C, \theta^C, u_1^D, u_2^D, \theta^D]^T$$
$$\alpha^4 = [u_1^D, u_2^D, \theta^D, u_1^E, u_2^E, \theta^E]^T$$
$$\alpha^5 = [u_1^E, u_2^E, \theta^E, u_1^F, u_2^F, \theta^F]^T$$

After the boundary conditions are applied, the reduced body nodal variable vector is

$$\alpha_{reduced} = [u_1^A, u_2^A, \theta^A, \theta^B, u_1^C, u_2^C, \theta^C, u_1^D, u_2^D, \theta^D, u_1^E, \theta^E, u_1^F, u_2^F, \theta^F, u_1^G, u_2^G, \theta^G]^T \quad (3.19)$$

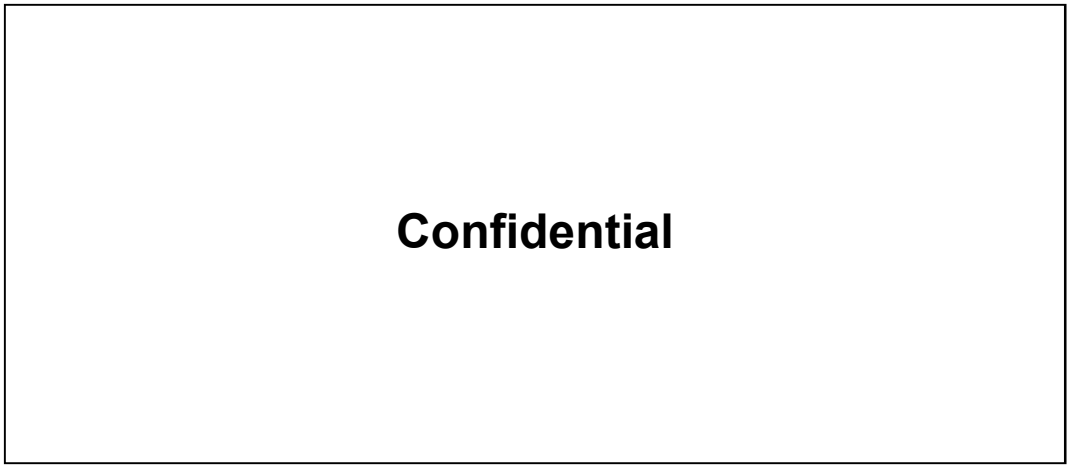

Figure 3.10: Boundary conditions and its positions

If we delete the columns and the rows restricted by the boundary conditions, the mass and stiffness matrices are reduced to 18x18 matrices.

Now, we can write undamped free vibration equation using the reduced mass and stiffness matrices.

$$\mathrm{M}\{\ddot{\mathrm{x}}\} + \mathrm{K}\{\mathrm{x}\} = 0 \quad (3.20)$$

If we solve the differential equation;

Let $\{x\} = \{X\}e^{-i\omega t}$ and so, $\{\ddot{x}\} = -\{X\}\omega^2 e^{-i\omega t}$

$$[-\omega^2 M + K]\{X\}e^{-i\omega t} = 0$$

Then,

$$[K - \omega^2 M]\{X\} = 0 \qquad (3.21)$$

The eigenvalue problem is solved to calculate the mode shapes and the natural frequencies. Finally, we find the mode shapes and the natural frequencies;

Table 3.1: Mode Shapes

	1	2	3	4	5	6	7	8	9	10	11	12	13	14	15	16	17	18
1	0,00	0,00	0,00	0,00	0,00	0,00	0,00	0,00	0,00	0,00	0,00	0,00	0,00	0,00	0,00	0,00	0,00	1,00
2	0,00	0,00	0,00	0,00	0,00	0,00	0,00	0,00	0,00	0,00	0,01	-0,01	-0,02	0,00	0,00	0,00	0,00	0,00
3	0,01	0,00	-0,14	-0,82	-0,43	0,87	0,75	0,46	-0,24	0,21	-0,57	0,46	0,73	0,00	0,00	0,00	0,00	0,00
4	0,00	0,00	0,00	0,00	0,00	0,00	0,00	0,00	0,00	0,00	0,00	0,00	0,00	0,00	0,00	0,00	0,00	0,00
5	0,00	0,00	0,00	0,00	0,00	0,00	0,00	0,00	0,00	0,00	0,00	0,00	0,00	0,00	0,00	0,00	0,00	0,00
6	0,01	0,00	-0,07	-0,39	-0,05	-0,12	-0,39	-0,42	0,24	-0,13	0,01	0,43	0,37	0,00	0,00	0,00	0,00	0,00
7	0,00	-0,04	0,00	0,00	0,00	0,00	0,00	0,00	0,00	0,00	0,00	0,00	0,00	-0,24	-0,59	-0,47	0,16	0,00
8	0,00	0,00	0,00	0,00	0,00	0,00	0,00	0,00	0,00	0,00	0,01	0,01	0,00	0,00	0,00	0,00	0,00	0,00
9	0,01	0,00	-0,06	-0,21	0,18	-0,32	0,19	0,51	-0,20	0,01	0,20	0,32	-0,06	0,00	0,00	0,00	0,00	0,00
10	0,00	0,11	0,00	0,00	0,00	0,00	0,00	0,00	0,00	0,00	0,00	0,00	0,00	0,37	0,37	-0,47	0,37	0,00
11	0,00	0,00	0,00	0,00	0,00	0,00	0,00	0,00	0,00	0,00	0,00	0,02	0,00	0,00	0,00	0,00	0,00	0,00
12	0,03	0,00	-0,07	-0,06	0,33	-0,09	0,39	-0,46	0,29	0,10	-0,35	-0,07	-0,23	0,00	0,00	0,00	0,00	0,00
13	0,00	-0,30	0,00	0,00	0,00	0,00	0,00	0,00	0,00	0,00	0,00	0,00	0,00	-0,45	0,22	0,21	0,51	0,00
14	0,00	0,00	0,00	0,00	0,00	0,00	0,00	0,00	0,00	0,00	-0,01	0,01	0,00	0,00	0,00	0,00	0,00	0,00
15	0,14	0,00	-0,17	0,02	0,45	0,21	-0,15	0,01	-0,27	-0,10	0,17	-0,38	0,22	0,00	0,00	0,00	0,00	0,00
16	0,00	0,63	0,00	0,00	0,00	0,00	0,00	0,00	0,00	0,00	0,00	0,00	0,00	-0,04	-0,21	0,43	0,53	0,00
17	0,00	0,00	0,00	0,00	0,00	0,00	0,00	0,00	0,00	0,00	0,00	0,00	0,00	0,00	0,00	0,00	0,00	0,00
18	0,46	0,00	-0,14	0,08	-0,41	-0,19	0,20	-0,24	-0,09	0,30	0,40	-0,42	0,32	0,00	0,00	0,00	0,00	0,00
19	0,00	-0,71	0,00	0,00	0,00	0,00	0,00	0,00	0,00	0,00	0,00	0,00	0,00	0,78	-0,65	0,58	0,55	0,00
20	0,00	0,00	0,00	0,00	0,00	0,00	0,00	0,00	0,01	0,02	0,01	-0,01	0,01	0,00	0,00	0,00	0,00	0,00
21	0,88	0,00	0,96	-0,35	0,55	0,20	-0,20	0,31	0,82	0,91	0,56	-0,42	0,36	0,00	0,00	0,00	0,00	0,00

The axial degrees of freedom are located at rows 1, 4, 7, 10, 13, 16, 19 but the fourth row which is axial DOF of the B point is fixed by the bearing. As seen from Figure 3.11, there are axial and nonzero 6 mode shapes. The columns 2, 14, 15, 16, 17 and 18 represent the axial mode shapes. The other columns are the bending mode shapes.

Table 3.2: Natural Frequencies

1	8,39E+06
2	7,44E+06
3	4,25E+06
4	3,94E+06
5	2,57E+06
6	2,04E+06
7	1,49E+06
8	9,95E+05
9	5,90E+05
10	4,05E+05
11	2,48E+05
12	4,84E+04
13	1,53E+05
14	4,18E+06
15	3,09E+06
16	1,75E+06
17	5,58E+05
18	2,60E+06

If we select the minimum natural frequency, we can calculate the maximum rotational speed;

$\omega_{\min}$ =4.84E+04 rad/s

$$n = 4{,}84\mathrm{E}+04 \ \frac{rad}{s}\frac{revolution}{2\pi}\frac{60s}{dk} = 46218 \ rev/\min$$

In practice, the shaft must work sufficiently below the speed. The motor driving the shaft rotates at 5000 rpm. Therefore, the speed is fairly safe.

3.3.2 Bearings

Bearings are one of the critical parts of thrust systems. If propeller shaft isn't supported sufficiently, the shaft may fail due to vibrations and even the propeller doesn't work efficiently. The propeller shaft is subject to thrust forces by both propeller and hydrostatic pressure.

Two radial ball bearings are used to support the shaft. Radial ball bearings can carry both thrust and radial loads. The shaft speed is about 5000 rpm and the radial bearings can work up to 24000 rpm. The static load rating of the radial ball bearing should be compared with the equivalent static load. According to the bearing catalogue [13];

$$P_o = 0.6F_r + 0.5F_a(kN)\,\frac{F_a}{F_r} > 0,8 \tag{3.21}$$

P_o : Equivalent static load

F_r : Radial load

F_a : Axial Load

The radial load is so low when we compare the load with axial load. Therefore, it is neglected.

The axial load due to hydrostatic pressure and propeller thrust force is

$$F_a = \textbf{Confidential}\, x9.81 + 30x10^5\, N/m^2\, x\pi(0.003)^2 = 0.129kN \tag{3.22}$$

Then, the equivalent static load is found as

$$P_o = 0.5F_a(kN) = 0,065kN \tag{3.23}$$

$$C_o = s_o P_o \tag{3.24}$$

C_o : Basic Static Load Rating

s_o : Safety Factor

The selected radial ball bearing dimension is 6x19x6 and it has 0.95kN basic static load rating. The bearings have also high fatigue life, although UUV will only work 8 minutes.

Finally, the equivalent static load is compared with the basic static load rating.

Safety Factor;

$$s_o = \frac{C_o}{P_o} = \frac{0.95}{0.065} = 14.6 \tag{3.25}$$

Two bearings are located to two both ends of the propeller shaft to decrease vibrations.

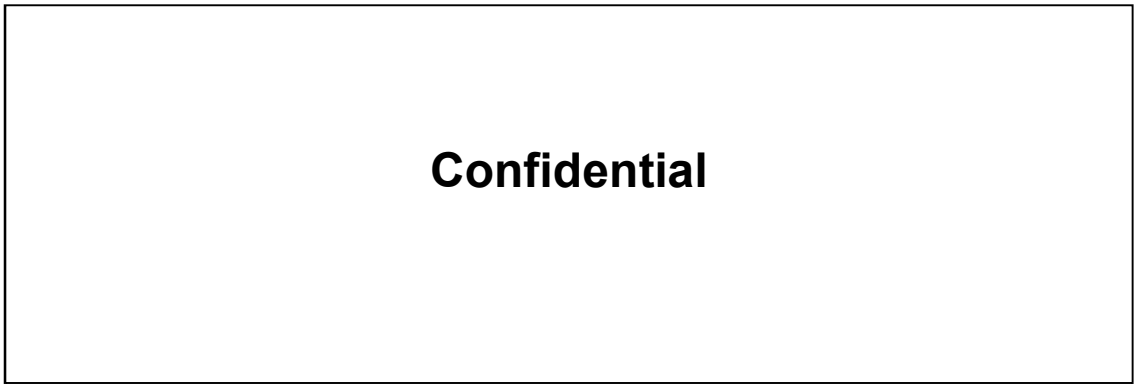

Figure 3.11: The propeller shaft, radial ball bearings and other thrust system parts

3.4 Sealing Elements and Design

The hull of target emulator must be dry and watertight. Because some equipment which are battery, motor, electronic cards can be impaired and can even burn due to leakage.

Therefore, we must use some materials or parts to isolate the body from water. There is mainly two types of sealing element is needed. The propeller shaft needs rotary shaft type seal. The other one should be used among static body parts. The sealing elements must protect the hull against water at the maximum working depth, h=300 m. We have found before the pressure value in equation (3.10) as 31.62 bar. The pressure doesn't require any special sealing elements for the static parts. Applicable sealing elements are liquid seals, gaskets, and O-rings for the static sealing. On the contrary, 31.62 bar is high for the standard rotary shaft type seals. The suitable elements for the rotary shafts which are mechanical shaft seal and lip seal.

The liquid seals are used in so many applications and there are available so many different types of them. They are directly applied to surface and don't need any grooves on the body. Although they are inexpensive and easily applicable, liquid seal application needs to be controlled. Therefore, the controlling can be performed by automation. Besides, UUV devices require flexibility and should be easy to assemble or disassemble. In addition, the liquid seals are not reusable and do need cleaning application surfaces.

Gaskets are widely used. The installation of gaskets are easy and simple, we can cut them to form desired solid shape. Nevertheless, the positioning of gaskets can create some leakage problems. They may also need cutting process. The main disadvantages of them are that they are deformed plastically.

O-ring, also known as, or a toric joint, is an elastic gasket in the shape of a torus. It is a loop of elastomer with a disc-shaped cross-section, designed to be seated in a groove and compressed during assembly between two or more parts, creating a seal at the interface [14]. They are inexpensive, reusable, easy to make, reliable, available in standard sizes and have simple mounting requirements. They can seal tens of megapascal pressure, because the O-rings are positioned within their grooves. The disadvantage of O-ring is that they need some grooves with close tolerances. Therefore, they bring extra cost of machining.

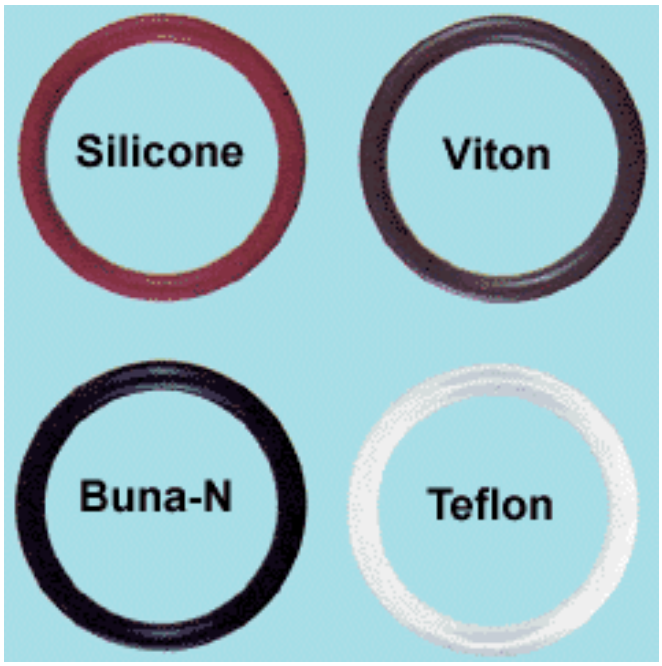

Figure 3.12: O-ring Types

Mechanical shaft seal is suitable for rotary shafts but it creates high friction surfaces between shaft and itself.

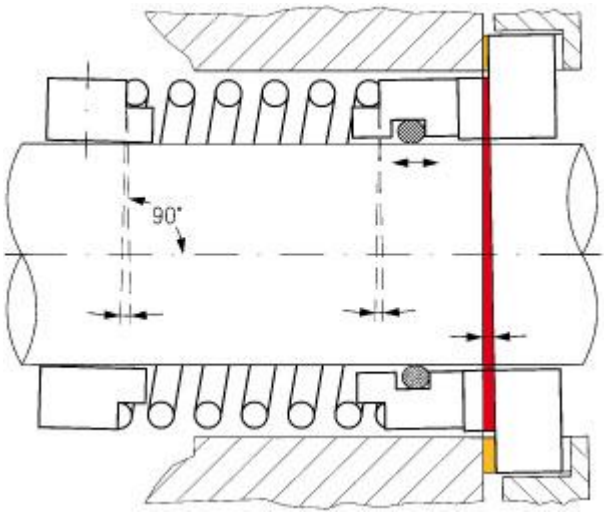

Figure 3.13: Mechanical Shaft Seal

Lip seal is an assembly consisting of a rubbing elastomer ring seal element held in place by spring. Besides, it has lips holding shaft and an O-ring on the outside diameter of the elastomer ring. The seal friction is reduced as an oil film is generated between lip of the seal and the shaft. Any damage to the shaft where the seal runs will cause leakage because the optimum oil film thickness will be exceeded locally. Therefore the shaft finish is especially important, as leakage will occur if an irregular surface is present. The lubricated rubbing provides the sealing action. This sealing action cannot be maintained at high speeds if the shaft is not running perfectly true. To maintain oil film thickness of the seal must follow any shaft movement. This becomes difficult when the shaft is subject to eccentric running or vibration at high speeds. Typically these seals will operate in the region of 18 m/s and the seals are affected by friction [15].

Figure 3.14: Lip Seal

3.4.1 Conclusion

We have selected O-ring as sealing element to seal static body parts. Because the cross section of the hull of UUV is circular. In addition, O-rings can be found easily in various sizes. They are reusable, so cheap, product of mass production and have low installation time. In addition, O-rings can be used in dynamic applications.

There are so many O-ring types with regard to their applications. So, we must select suitable the type to satisfy environmental and other conditions. The conditions are temperature, pressure, hardness, fluid medium and etc. Consequently we have selected O-ring which is nitrile rubber (NBR or Buna-N) having 70 shore hardness. The temperature range is between -40°C and 135°C. Besides, we have designed groove of O-ring which is called as gland area and the piston type seal is selected.

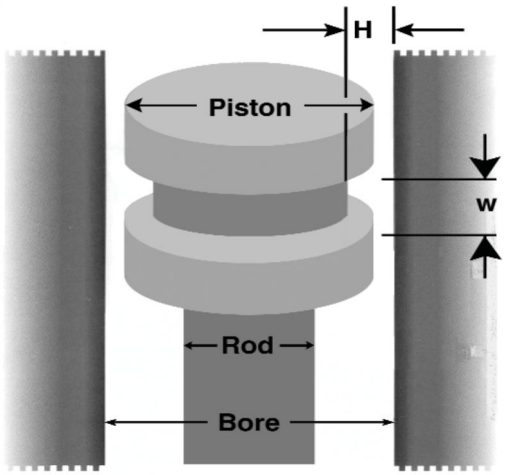

Figure 3.15: The Piston Type Seal

The ratio between gland diameter and O-Ring ID should be maximum 2%.

The compression ratio and gland fill are the most important factors during the gland design. We have selected %20 compression ratio and % 75 gland fill. Besides, a clearance must be held between mating piston and bore parts and for installation. Nevertheless, so large clearance can result in extrusion of O-rings at high pressures.

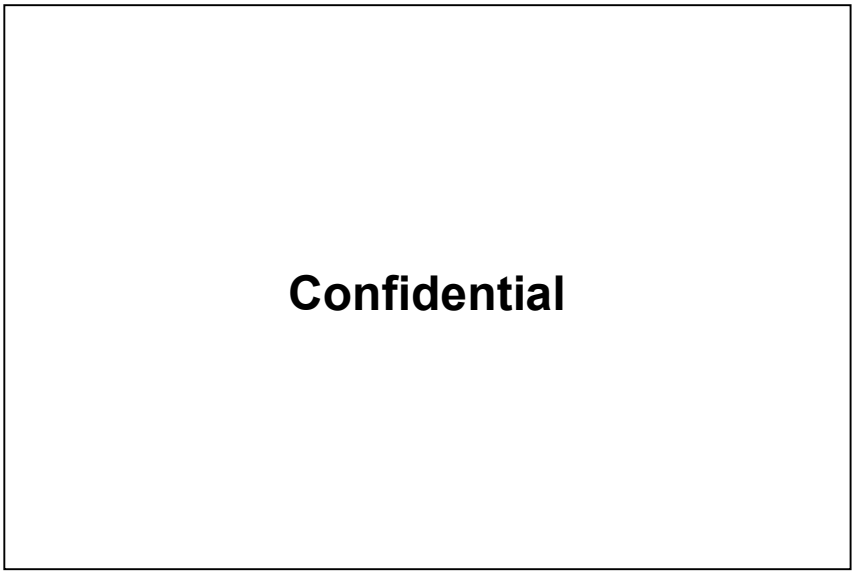

Figure 3.16: Design of gland area of O-ring

We have chosen the lip seal to seal the shaft of propeller. However, we could not find any standard seal with spring which works at 31.6 bar in Turkey. Thus, we have designed and manufactured special teflon lip seal for the rotary shaft. The manufactured seal have an outer O-ring and lips which are placed inside diameter. The inner diameter of the seal is held in minimum to reduce the friction.

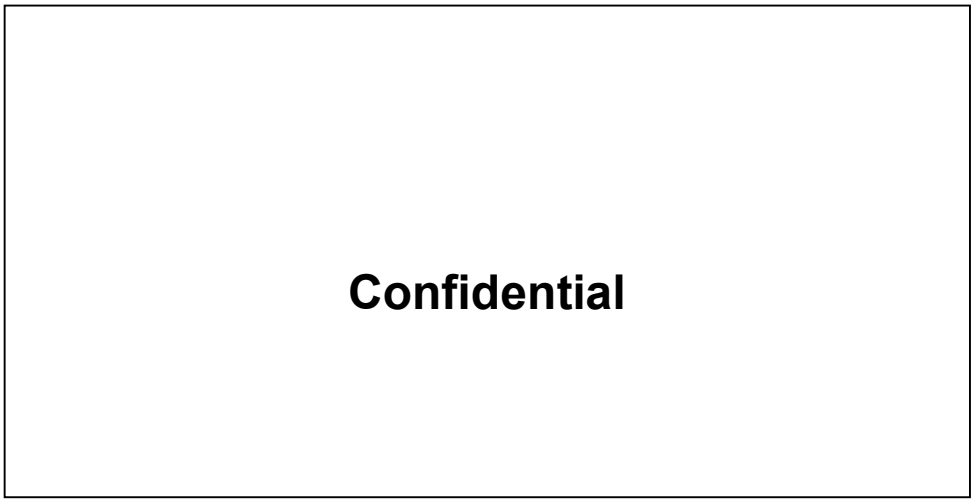

Figure 3.17: Location of Lip Seal on Shaft

3.4.2 Leakage Test

We have carried out some leak tests to ensure whether the lip seal prevents leakage or not. The target emulator is submerged into a water tank to test the lip seal. The tank can be pressurized by means of hand or hydraulic pump. The pressure of water tank have increased from 0 bar to 5MPa and inversely decreased from 5MPa to 0 bar during tests. Furthermore, the friction between the lip seal and propeller shaft is measured at different motor speeds in that test.

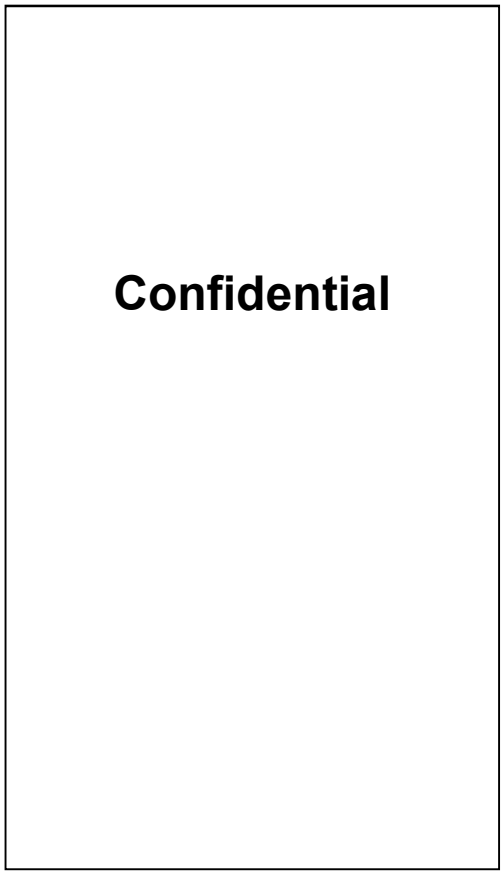

Figure 3.18: Leak Test Setup

Confidential

Figure 3.19: Detailed View of Leak Test Setup

Figure 3.20: Leak Test

3.4.2.1 Results of Leakage Test

The tests are performed successfully and it is observed that the lip seal hasn't permitted any leakage.

In addition, some results are obtained.

- There is no leakage up to 5MPa which is highest test pressure
- 8 pieces of M3 bolts are enough to compress the O-rings to prevent leakage
- 10-15% O-ring compression ratio is sufficient to prevent leakage.
- The diameter of propeller shaft affects the friction between the lip seal and propeller shaft. The smaller inside diameter of lip seal is, the smaller it creates friction moment. Thus, we have tested the lip seals having different inside diameters. The diameters are **Confidential** mm. Finally, we have selected the **Confidential** of inside diameter lip seal. The seal hasn't permitted any leakage during tests.
- Different interference values between the shaft and lip seal having 6 mm inside diameter are also tested to optimize the power loss due to friction.

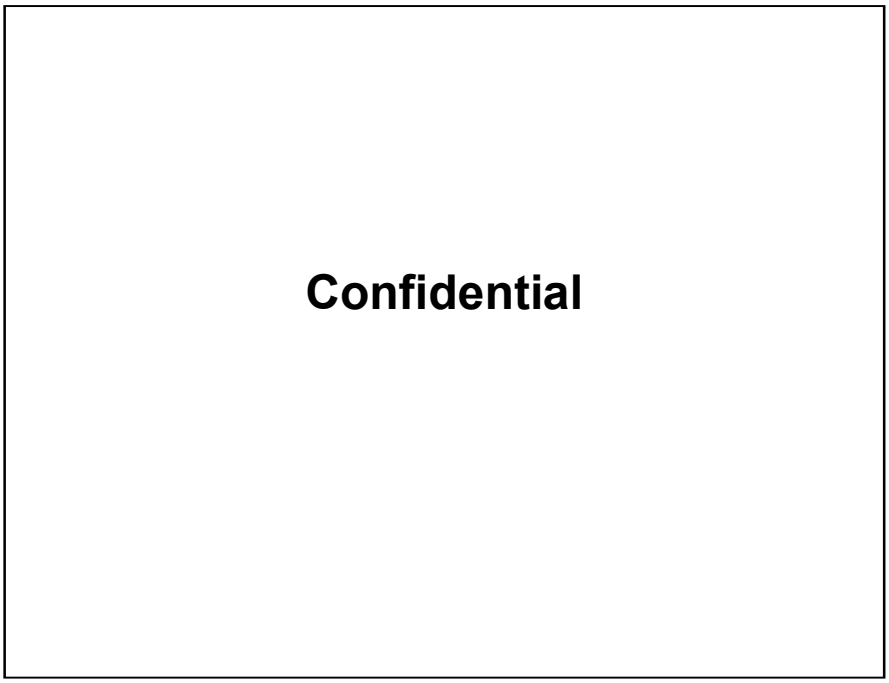

Figure 3.21: Comparing power consumption of the different interference values between shaft and lip seal

The power consumption is increased while the interference value is increased according to Figure 3.21. This means that the power loss increases as the interference value increases. Thus, we should select the minimum interference value. Nevertheless, it is also observed that the lip seal having **Confidential** interference value has leaked, whereas the lip seals having **Confidential** and **Confidential** interference values haven't leaked. Consequently, the **Confidential** of interference value is selected with a sufficient margin of safety.

3.5 Anti Roll Fins and Eccentric Weights

The roll moment produced by propeller must be prevented to control decoy. Two methods are available to reach this aim. They are anti-roll fins and eccentric weights. Eccentric weights increase energy consumption due to extra weight. Therefore, some equipment is located inside of the UUV as eccentric to create anti-roll effect without extra weight.

However, the anti-roll effect isn't enough to prevent the roll movement. The anti-roll fins are also used to balance the roll moment. The required anti-roll moment for the anti-roll fins is calculated as following;

There is **Confidential** of eccentricity of the centre of mass of UUV due to the equipment located as eccentric. The eccentricity creates anti-roll moment for the UVV which is 8 kg.

$$M_{eccentric} = mR_{eccentric} \quad (3.25)$$

$$M_{eccentric} = \textbf{Confidential} \quad (3.26)$$

The required anti-roll moment for anti-roll fins;

$$M_{fins} = M_{roll} - M_{eccentric} \quad (3.27)$$

$$M_{fins} = \textbf{Confidential} \quad (3.28)$$

3.5.1 Anti-Roll Fins

When decoy goes with a certain speed, anti-roll fins create a counter moment which depends on the UUV speed. The moment helps preventing the roll moment.

The anti-roll fins are designed according to the CFD design team of the project and they are located on the duct of propeller. The fins create about **Confidential** anti-roll moment according to the CFD results.

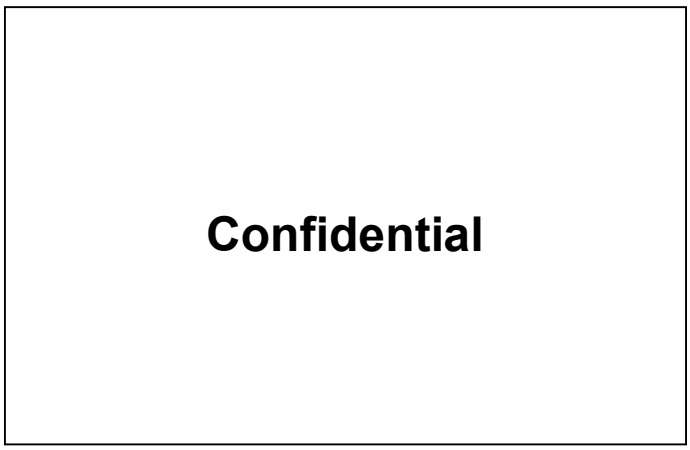

Figure 3.22: The anti-roll fins and the duct of propeller

3.5.2 Eccentric Weights

The eccentric weights are designed and located at the inner side of cylinder body of UUV to simulate the effect of the eccentric equipment. Thanks to ropeway tests, it is also tested whether the anti-roll moment created by the eccentric equipment and anti-roll fins are enough.

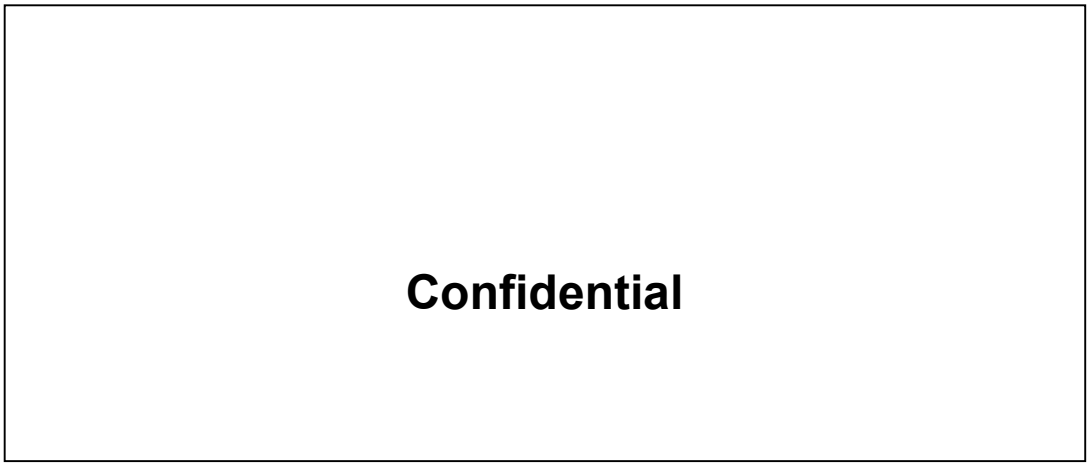

Figure 3.23: Eccentric weights.

There is 36 mm offset between the UUV and the designed eccentric weight mass centres. The required amount of eccentric weight is calculated to simulate the effects of eccentric equipment as following;

$$m_{weight} = \frac{M_{eccentric}}{R_{weight}} \tag{3.29}$$

$$m_{weight} = \textbf{Confidential} \tag{3.30}$$

m_{weight} = **Confidential** (3.31)

3.6 Ropeway tests

In ropeway tests, it is aimed to measure that the speed of UUV and the roll moment created by propeller. For that purpose, the UUV body is supported by two radial ball bearings at the both ends to observe the roll movement. The bearings are hung from two ropes connected to an apparatus via hooks.

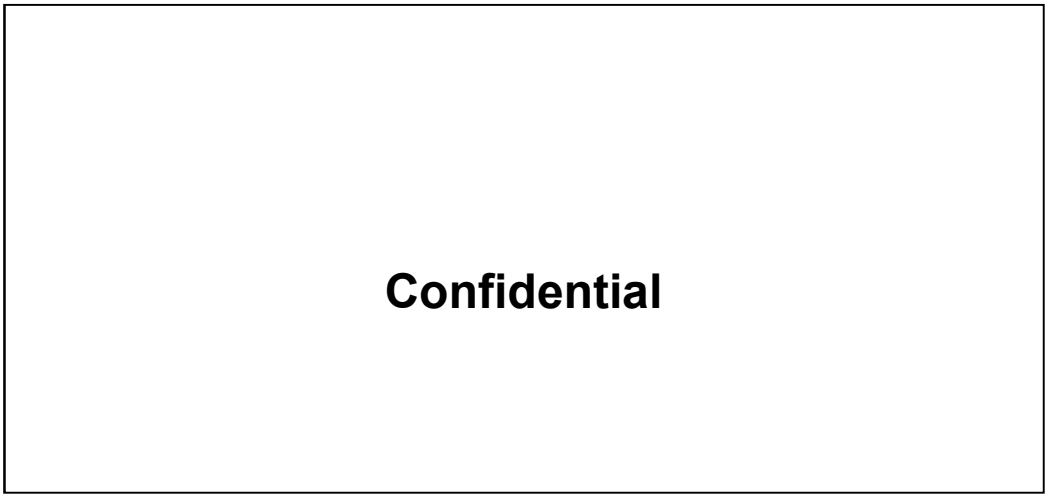

Figure 3.24: Front view of the ropeway test setup

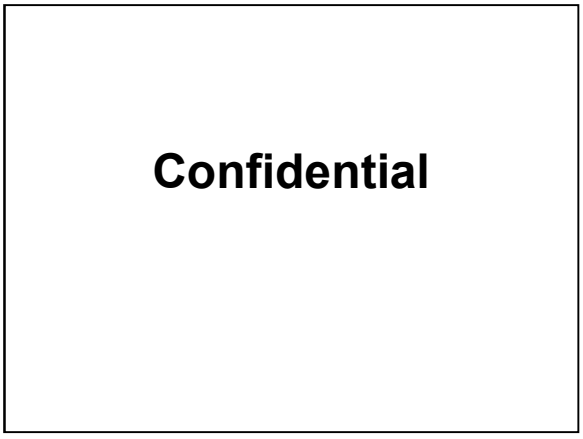

Figure 3.25: Isometric view of the ropeway test setup

The apparatus also two rolling bearings moving on stretched steel wire rope. When the bearings move axially on the stretched steel wire rope, they aren't allowed to spin thanks to

weight of the UUV (Positive Buoyancy). The speed and roll tests are performed by using the test setup.

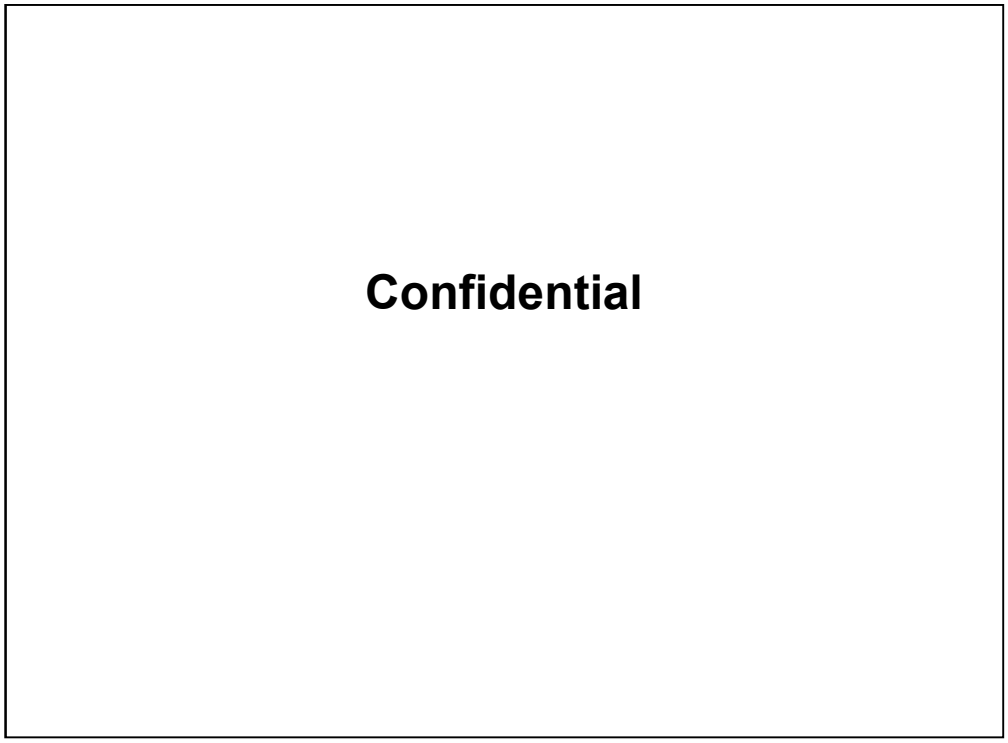

Figure 3.26: The ropeway test system

3.6.1 Conclusions

Table 3.3: The important ropeway test results

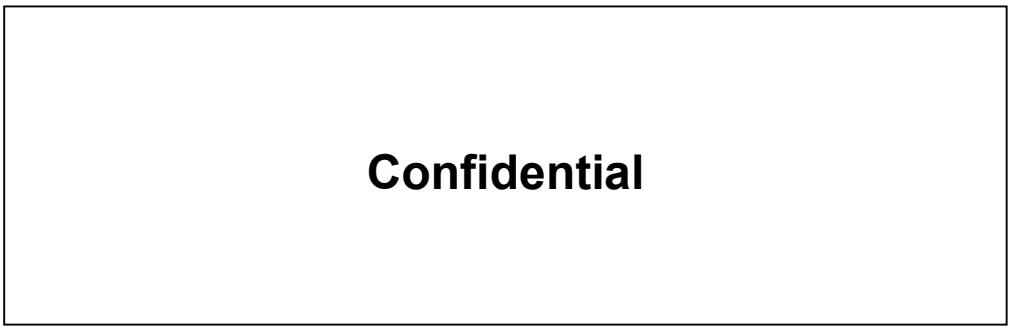

After many tests, we get some results about the propeller performance in the ropeway tests. The important results are given in Table 3.3. According to the table, the UUV's speed has reached speed of **Confidential** (about **Confidential**) at 4740 rpm of motor speed. However, the maximum allowable roll angle is **Confidential** for the electronic equipment. The desired thrust force is obtained by the propeller at 4740 rpm while the roll moment (**Confidential**°) is high. It means that the propeller hasn't the required propeller performance. Thus, a new propeller design is made to obtain lower roll moment at speed of **Confidential**. The new design propeller is tested again in the ropeway test setup and the roll-thrust performance (propeller performance) is obtained in Table 3.4.

Table 3.4: The test results of new propeller design

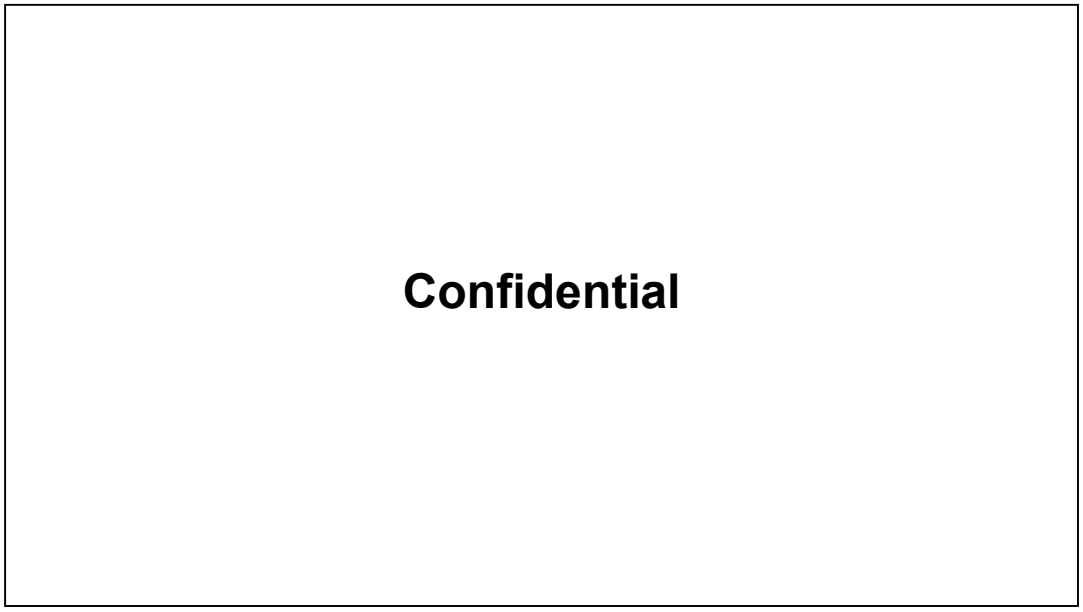

According to the Table 3.4, we have reached speed of **Confidential** at 4800 rpm of motor speed with **Confidential** of roll angle. Furthermore, the maximum UUV's speed is **Confidential** m/s (about **Confidential**) at 5640 rpm with **Confidential**.

3.7 Stability and Stability Fins

After the UUV is launched from the submarine signal ejector, the device is unstable due to turbulences caused by high velocity. To improve the stability of decoy, some stability fins are designed and placed on the conical side of UUV. The stability fins are more effective when they are located at the back side. Firstly, the cross section of stability fins was rectangular to be used for the preliminary tests. Then, the cross section is designed as hydrodynamic and thanks to that improvement, the drag force of decoy is decreased. Two alternatives of the stability fins are designed according to the CFD design team of the project.

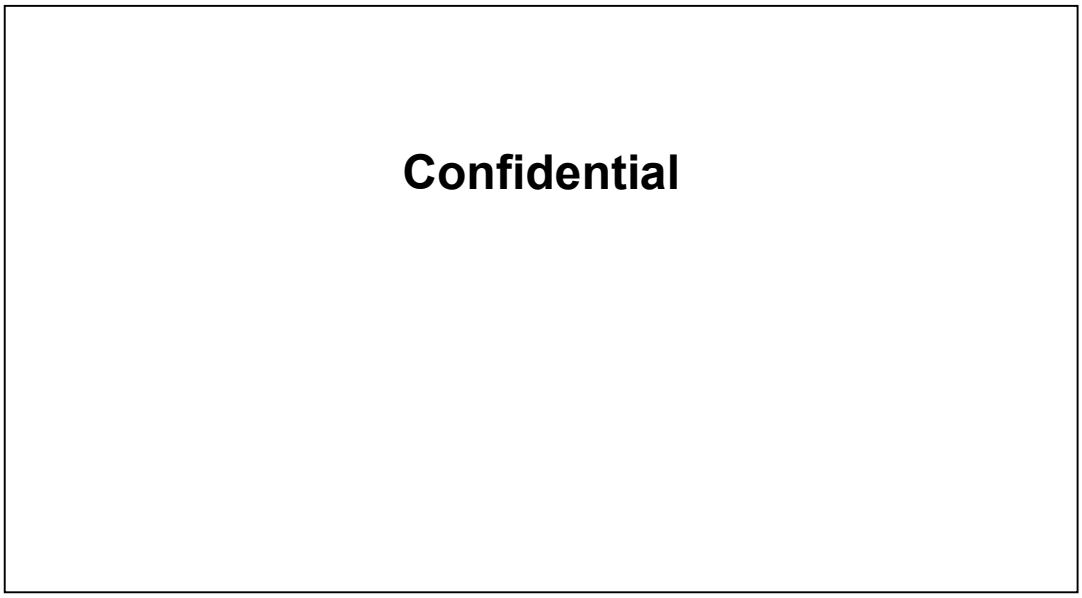

Figure 3.27: Two alternatives to stability fin

Some stability tests are made to whether the decoy is stable or not after the launch. Furthermore, the other aim is to decide which stability fin is more effective. Therefore, a test setup is designed and constructed to launch the decoy at different angles.

3.7.1 Adjustable Ejector Test Setup

Adjustable ejector is used to test movements of the decoy during ejection. Thanks to the adjustable signal ejector, it is observed the effects of anti-roll fins, eccentric weights and stability fins. The device can be adjusted to different azimuth angles, because it is desired that the ejector simulates different type of submarine signal ejectors (SSE). The maximum angle is 80 degrees and the minimum angle is 5 degrees. It is made of stainless steel to prevent the oxidation while the ejector is submerged into sea water.

3.7.1.1 Mechanism Design and Calculations

A slider-crank mechanism is designed to adjust angle of the ejector. According to the previous project works, it is observed that the air pressure created maximum 100g acceleration on the decoy during launch. Whereas the decoy was about 4.5 kg, the current decoy is about 8 kg. Thus, the acceleration is lower than 100g and the acceleration creates a reaction force on the ejector and adjustable ejector test setup parts.

$$A_{decoy} = \frac{100gx4.5kg}{8kg} = 56.25g \tag{3.32}$$

The reaction force due to the acceleration;

$$R = 56.25gx8kg = 4415N \tag{3.33}$$

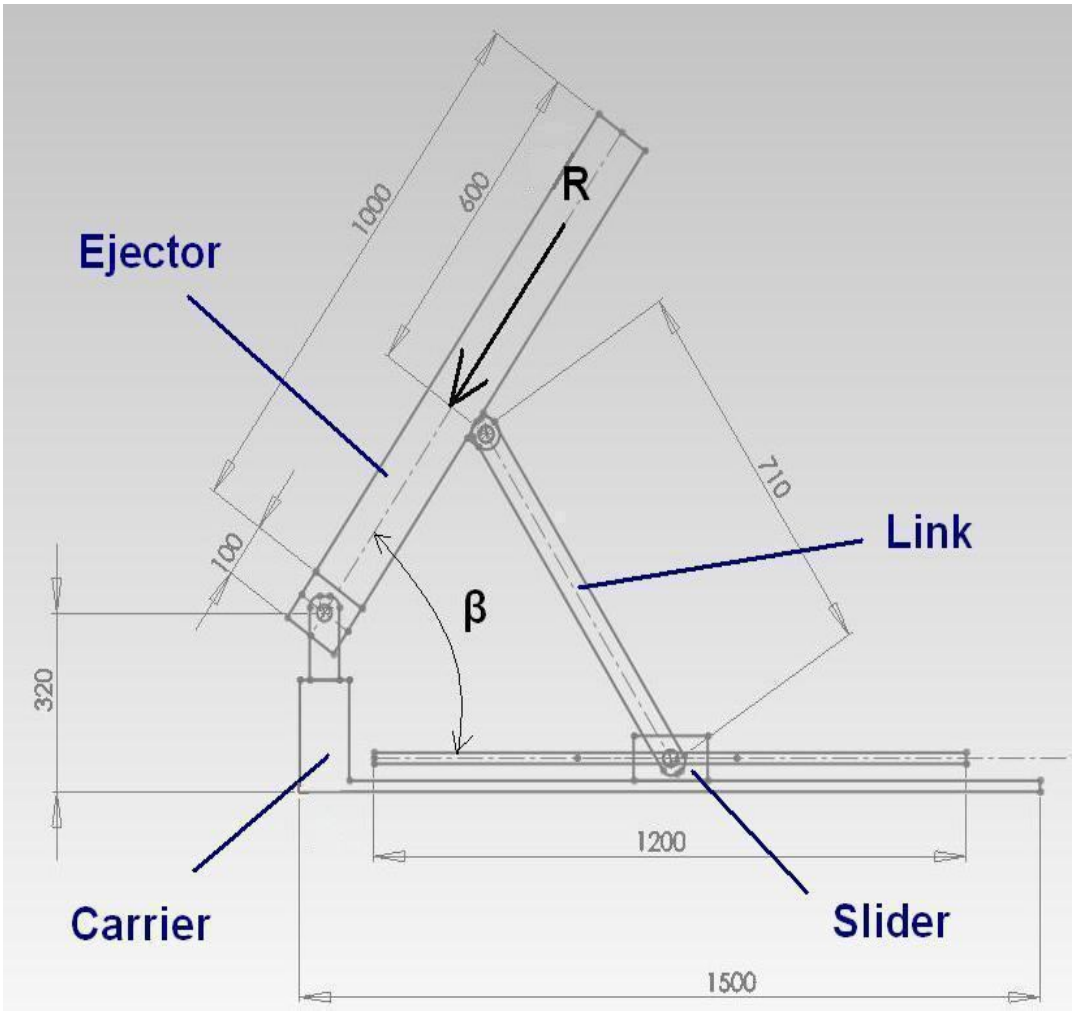

Figure 3.28: Slider crank mechanism of adjustable ejector

The adjustable ejector must be durable at different angles. Thus, the construction must be designed according to the extreme load cases.

If we draw free body diagrams of the adjustable ejector at 80 and 5 degrees respectively, we get following figures;

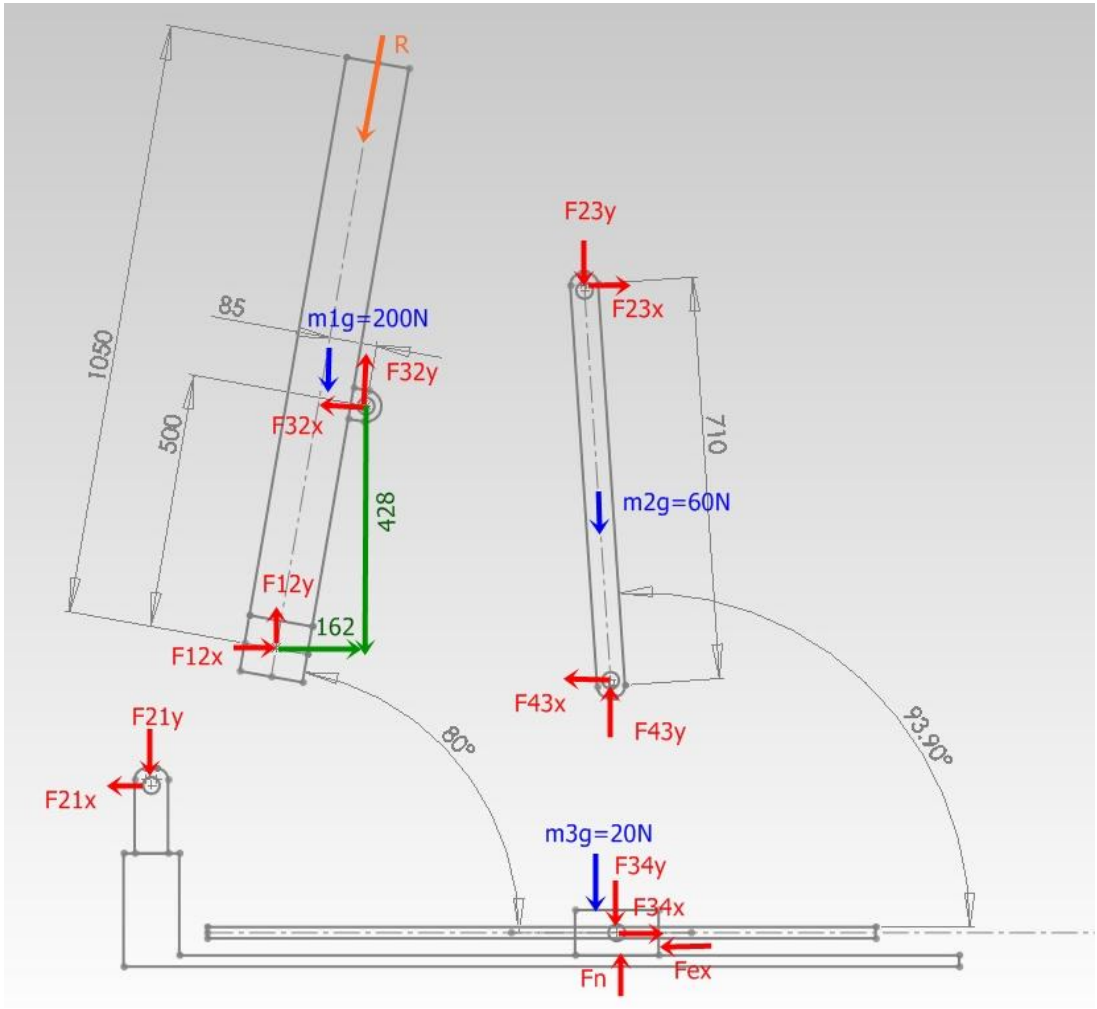

Figure 3.29: Free body diagram of adjustable ejector at 80 degrees

We have the 8 unknown forces and 8 equations. After solving the 8 equations, we find the forces.

$F_{12x} = 775N$

$F_{12y} = 4457.69N$

$F_{23x} = F_{32x} = 8.41N$

$F_{23y} = F_{32y} = 8.41N$

$F_{43x} = 8.41N$

$F_{43y} = 150.31N$

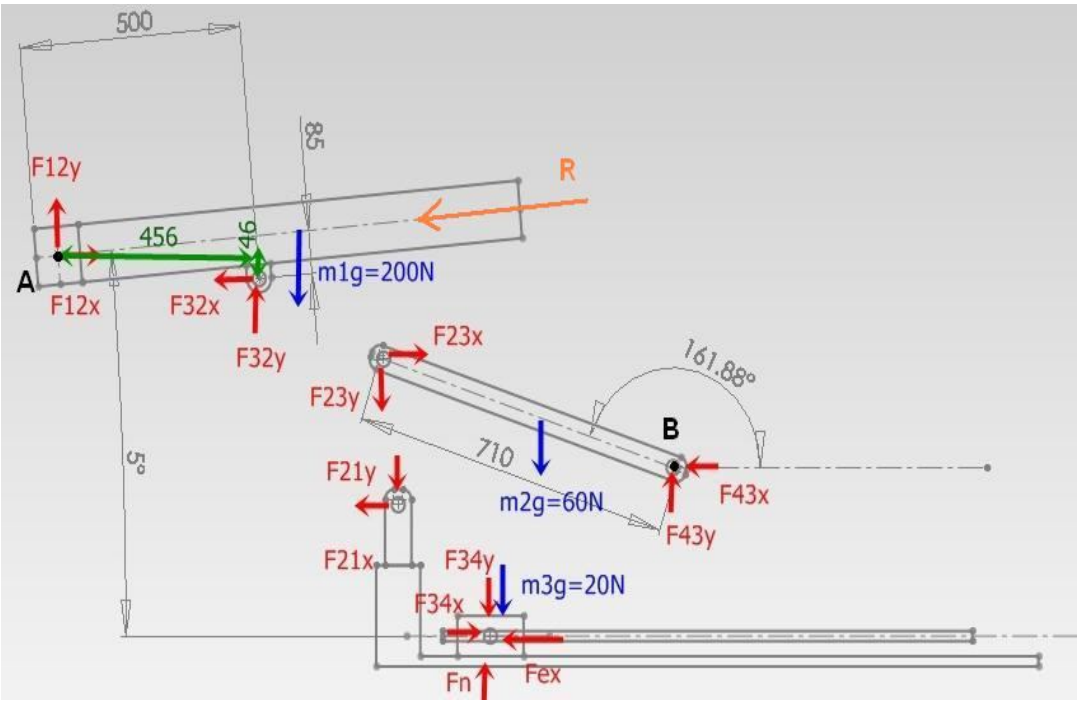

Figure 3.30: Free body diagram of adjustable ejector at 5 degrees

We have the 8 unknown forces and 8 equations. After solving the 8 equations, we find the forces.

$$F_{12x} = 5570N$$
$$F_{12y} = 237N$$
$$F_{23x} = F_{32x} = 1172N$$
$$F_{23y} = F_{32y} = 348N$$
$$F_{43x} = 1172N$$
$$F_{43y} = 408N$$

We have also calculated the minimum diameter of pin between the ejector and carrier. The pin should endure the shear stress created during launch.

$$F_p = 39270N$$
$$\tau_{alllowable,steel} = 100Mpa$$

$$\tau_{alllowable,steel} = \frac{F_p}{r_{\min}} \tag{3.34}$$

$\rightarrow r_{min} \approx 11mm$

We have selected the pin diameter as 65 mm.

Thanks to above all calculations, the adjustable ejector is constructed and manufactured as following figures;

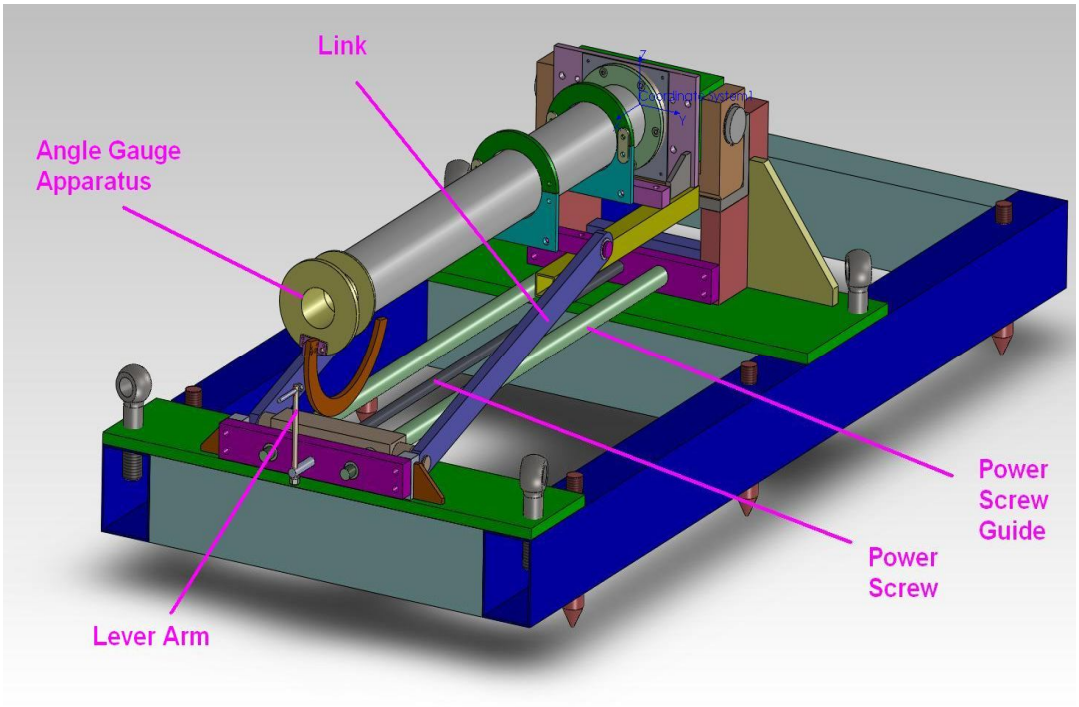

Figure 3.31: Isometric view of the adjustable ejector

The angle of ejector can be changed with a lever which is connected to a M20 power screw. The power screw can move slider and the slider move up or down the ejector. The ejector has also angle gauge apparatus to adjust desired angle correctly. The apparatus has a part having notches to designate certain angles. The apparatus is removed before decoy is launched.

Figure 3.32: The manufactured adjustable ejector

The ejector has a pneumatic launching system to launch the UUV under the sea. The pneumatic diagram of launching system is also as following figure;

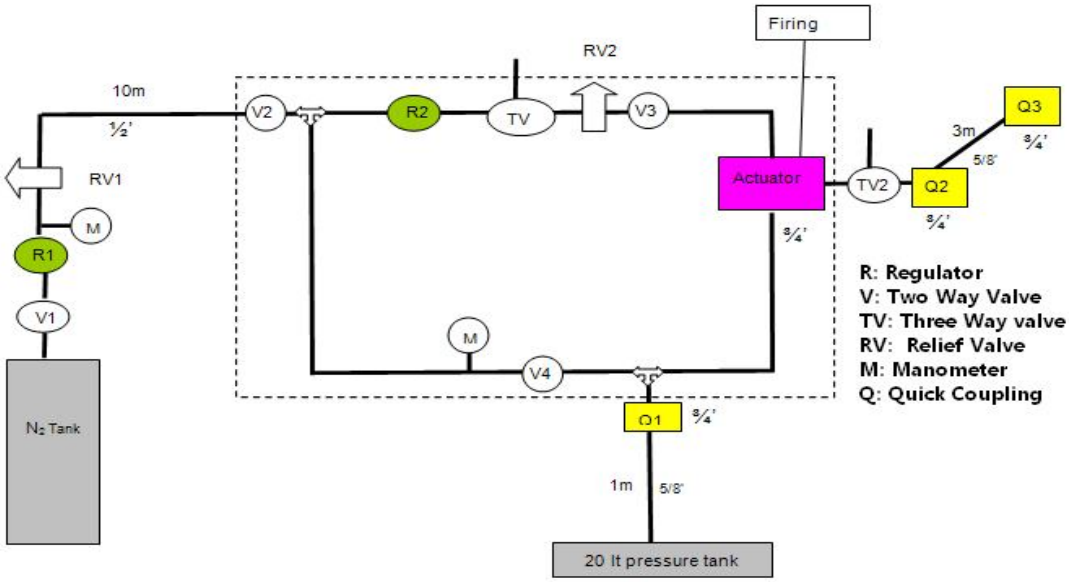

Figure 3.33: Pneumatic diagram of launching system

3.7.1.2 Test Results

The adjustable ejector is manufactured and stability tests are made at different angles. Finally, it is observed that the UUV is stable and the first alternative of stability fins is more effective. Furthermore, the anti-roll fins don't create instability after the launching.

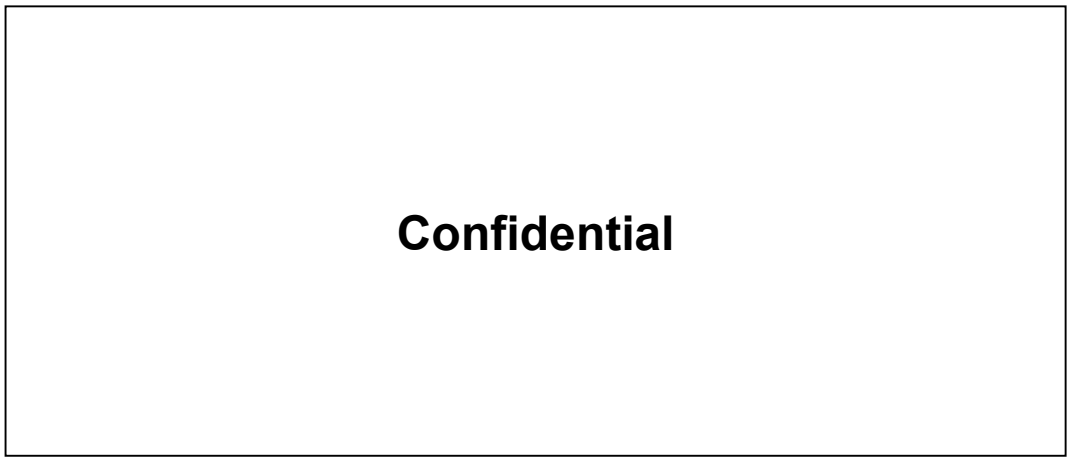

Figure 3.34: The stability fins and its location on the UUV

CHAPTER 4

CONTROL FIN SYSTEM

4.1 Control Fin System

It is desired that UUV can move in all directions. Thus, a control fin system is required to move the UUV. The UUV is controlled via two control fins to move up, down and left and right the target emulator. Two alternative control fin mechanisms are designed to move the control fins.

4.1.1 Alternative 1: Solenoid Control Fin System

Solenoids are used to move the control fins in the mechanism. The solenoid is a coil wound into a tightly packed helix. They are transducer devices that convert the magnetic energy into the linear motion.

Solenoids must be watertight as they should work in the water. However, it creates a disadvantage, because the solenoid isolated from water can be easily heat up.

The control fins must rotate **Confidential** to give required manoeuvres to the UUV according to the CFD design team of the project. To do that, the solenoids must move sufficiently.

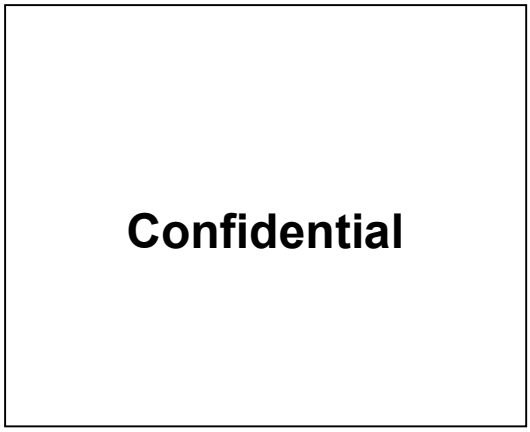

Figure 4.1: The selected watertight solenoid

In this system, the solenoid shaft pushes a pin and the pin press to the lug of the control fin. Then the control fin rotates at its axis. In the end, the UUV rotates to the direction which is same as the fin direction due to drag force.

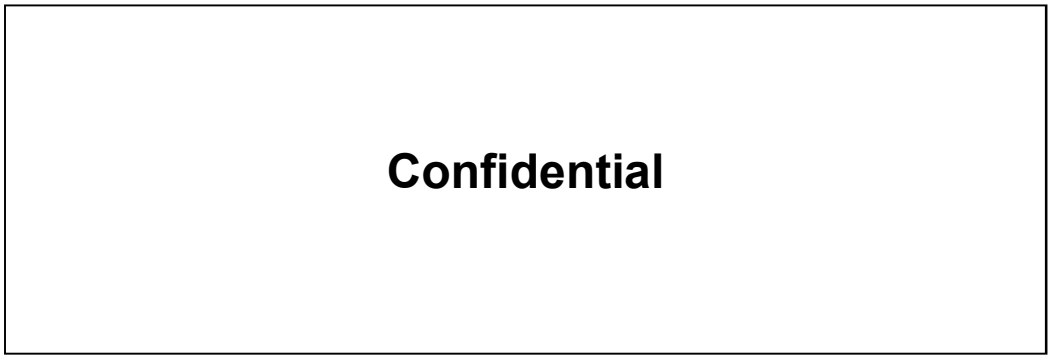

Figure 4.2: Solenoid Control Fin System

Each control fin has two solenoids to turn left and right or up and down each one. While the pin presses the control fin lug and the control fin rotates, the other lug presses the opposite pin backwards. If the opposite pin touches to the solenoid shaft, the control fin can't rotate sufficiently. Therefore, there must be minimum gap between the pin and solenoid. The amount of minimum gap depends on the angle of rotation.

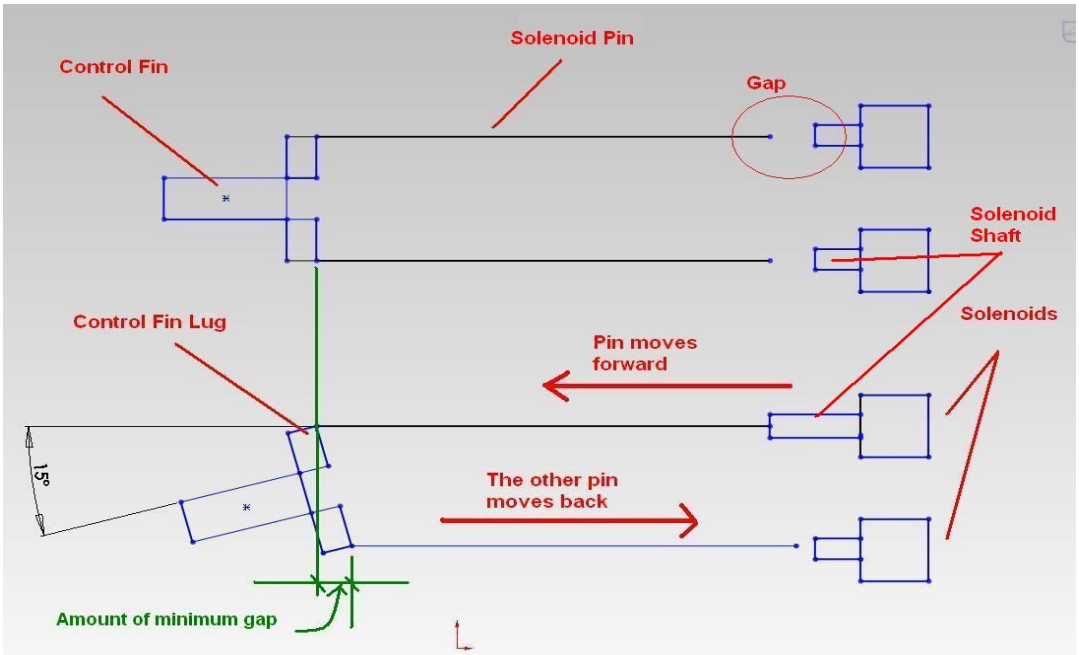

Figure 4.3: Solenoid Pin Mechanisms

Furthermore, springs and stops are located on the UUV body. The springs are used to retract the solenoid shafts when the solenoids are powered off. The stop determines the end point when the solenoid shaft retracts.

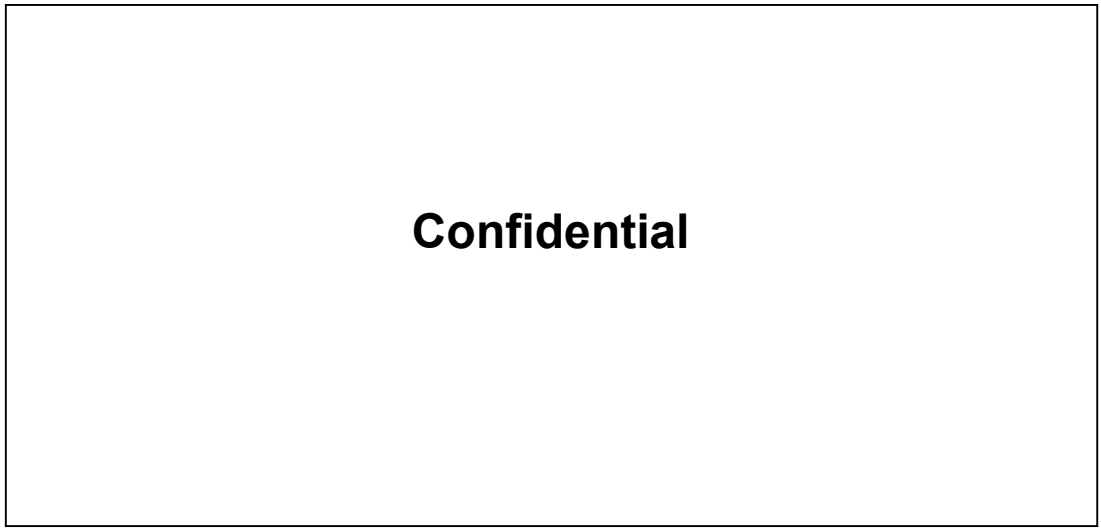

Figure 4.4: Detailed Solenoid Control Fin System

The solenoid pin length and gap are calculated according to following figure;

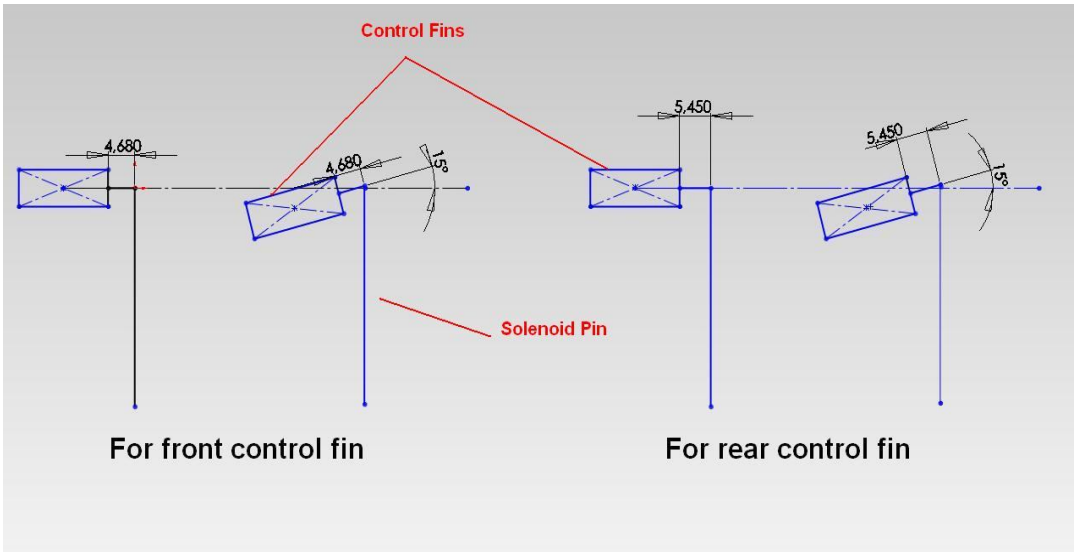

Figure 4.5: The calculation of minimum gap for front (blue) and rear (yellow) control fins

If we accept that 15 degree is small we can find the gaps approximately which are equal to the vertical distances above figure.

$$X_{gap,front} = 4.68 \sin 15 = 1.21 mm$$
$$X_{gap,rear} = 5.45 \sin 15 = 1.41 mm$$

The maximum stroke of solenoid shaft is **Confidential**. Each gap is smaller than **Confidential**. Therefore, that design is suitable.

4.1.2 Alternative 2: Mini Motor Control Fin System

The other alternative is designed to improve the mechanical efficiency. The system generally consists of two mini motors. Each mini motor controls each control fin. However, it is required also extra sealing elements for each mini motor to prevent the leakage.

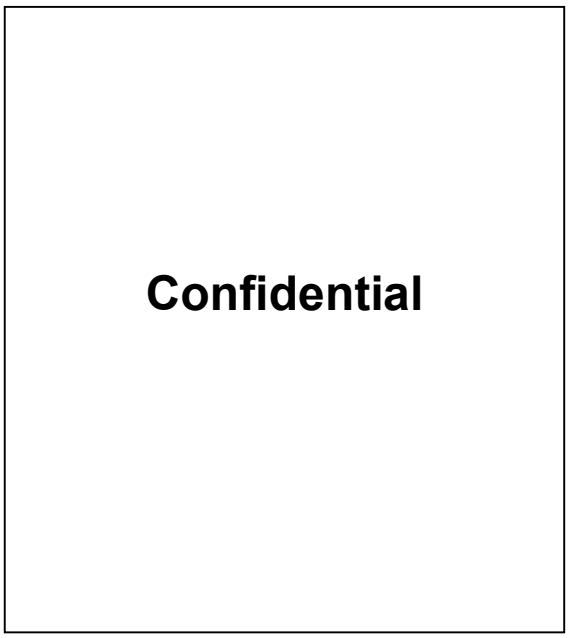

Figure 4.6: 12 mm Mini motor

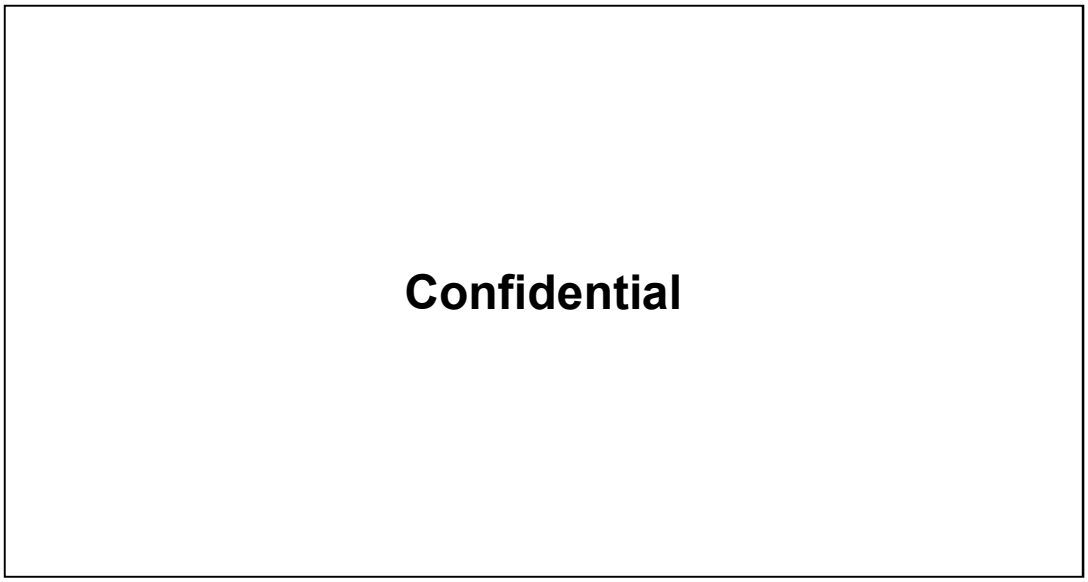

Figure 4.7: Mini motor Assembly

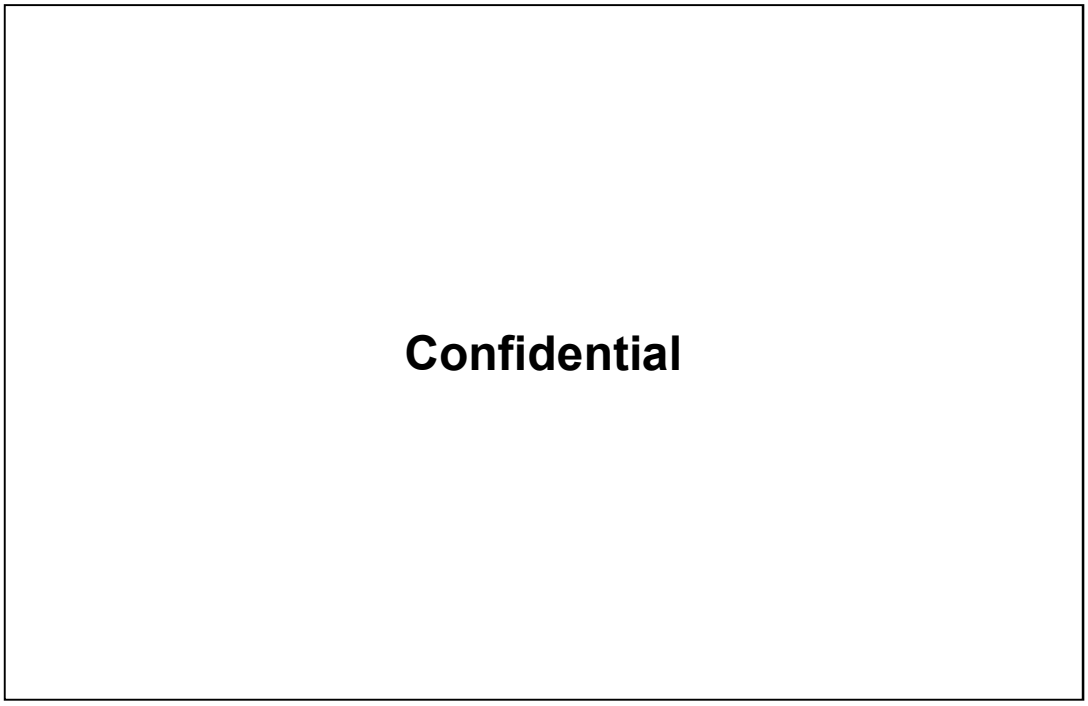

Figure 4.8 Mini motor assembly parts

The fins and mini motor are connected to each other via some pins. When the mini motor shaft moves forward or backward, the pins rotate the control fins.

4.2 Conclusions

- Two systems are designed and manufactured and they are compared.
- The mini motor system is more efficient and precise
- The solenoid system needs 4 solenoids, whereas the mini motor system requires 2 mini motor.
- The mini motor system is more complicated when compared with the solenoid system. It consists of so small parts which can't be machined easily.
- The mini motor requires two extra sealing elements to prevent the leakage from mini motor shafts.

In conclusion, the solenoid system is more reliable and having low cost. Mini motors consume less power but the mini motor sealing elements create extra friction losses. Finally, the solenoid control fin system is selected.

CHAPTER 5

FINITE ELEMENT ANALYSIS OF HULL

Finite element analysis is made to verify the calculations at Chapter 3 and calculate the stresses more accurately. Target emulator is analysed at extreme load case. In this case, the maximum launch acceleration (54.25g) and the maximum hydrostatic pressure (30bar) are taken into consideration.

Finite element analysis is performed via computer software. The software is ANSYS Workbench. Static structural analysis will be performed.

The target emulator analysis geometry is about 8 kg. The geometry consists of hull whose material is **Confidential**, battery and motor which is structural steel. The bolt, pin holes are closed to simplify the geometry for analysis. The analysis geometry is presented at Figure 5.1.

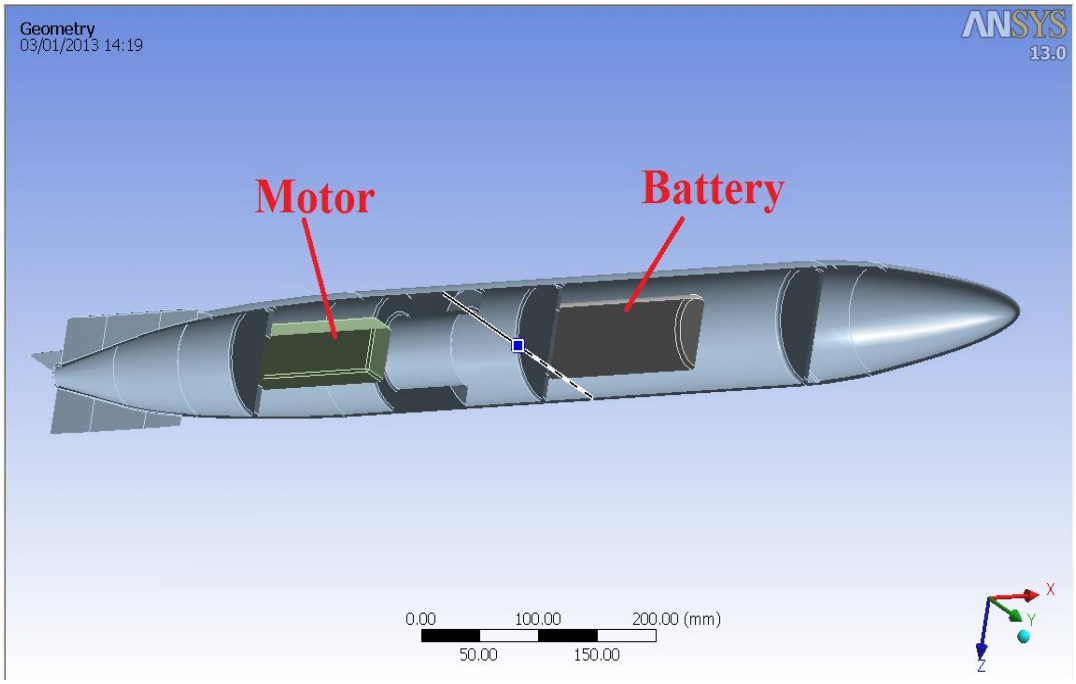

Figure 5.1: Finite Element Analysis Geometry

The geometry meshed with 1058744 tetrahedral elements which are in 1.5 mm size and 2273376 nodes. Then, contact faces are created among the hull-motor and hull-battery.

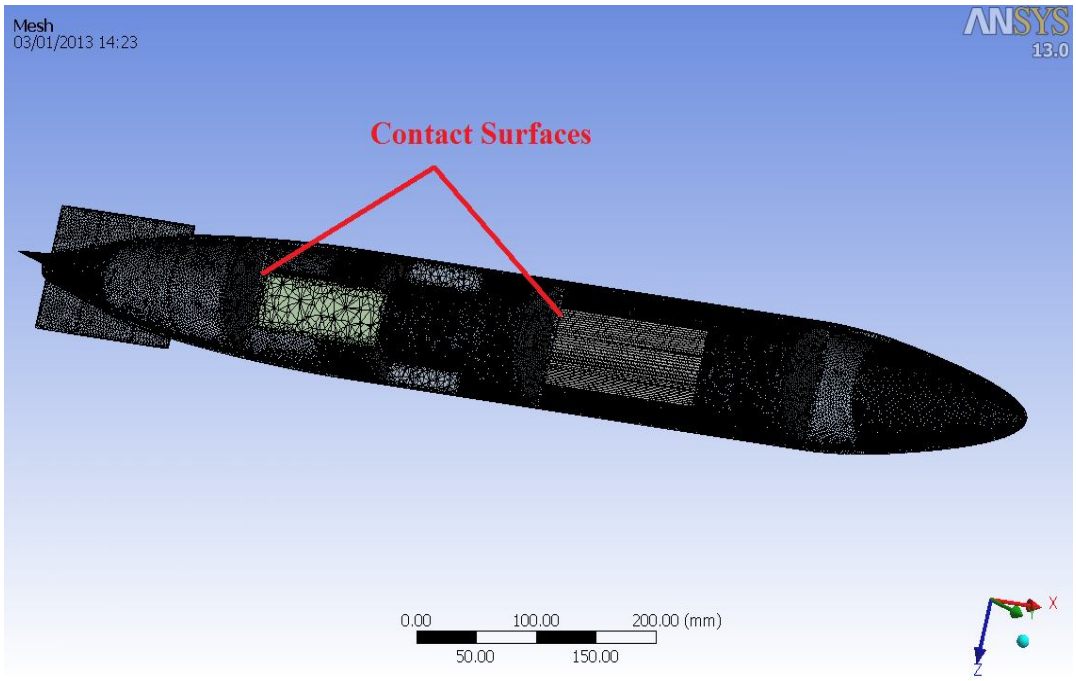

Figure 5.2: Meshed Geometry and Contact Faces

5MPa pressure is applied to back the side of the decoy during the launch and the pressure generates an acceleration on the decoy which is 54.25g.

In static analysis, the target emulator is fixed at the back side and the acceleration is specified as 54.25g in the opposite motion direction to simulate the load case statically. Therefore, the specified acceleration creates inertial forces in the same direction of the decoy's motion. The forces create reaction forces on the fixed side of the decoy. By using the configuration, the reaction forces represent the forces generated by the pressure of SSE during the launch. The configuration is shown in the Figure 5.3

Besides, the acceleration and hydrostatic pressure are specified at the same time in the FEA. The analysis shows the worst case while decoy is launched.

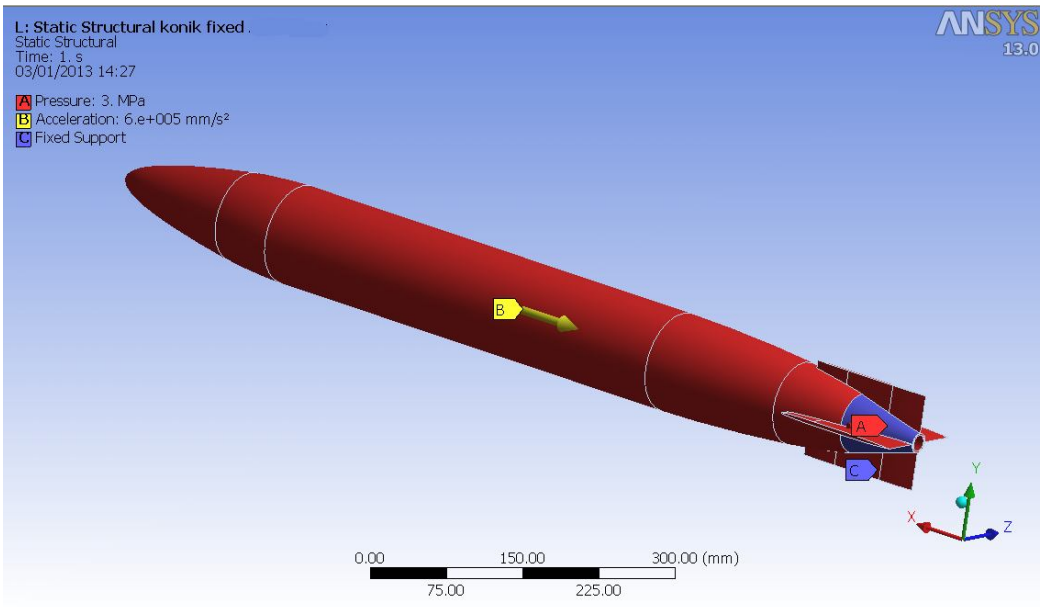

Figure 5.3: Loads, Direction of Acceleration and Boundary Conditions

Finally, the analysis is finished and the results are obtained. The results are presented in terms of equivalent (von-Mises) stresses and total deformations in Figure 5.4 and Figure 5.5 respectively.

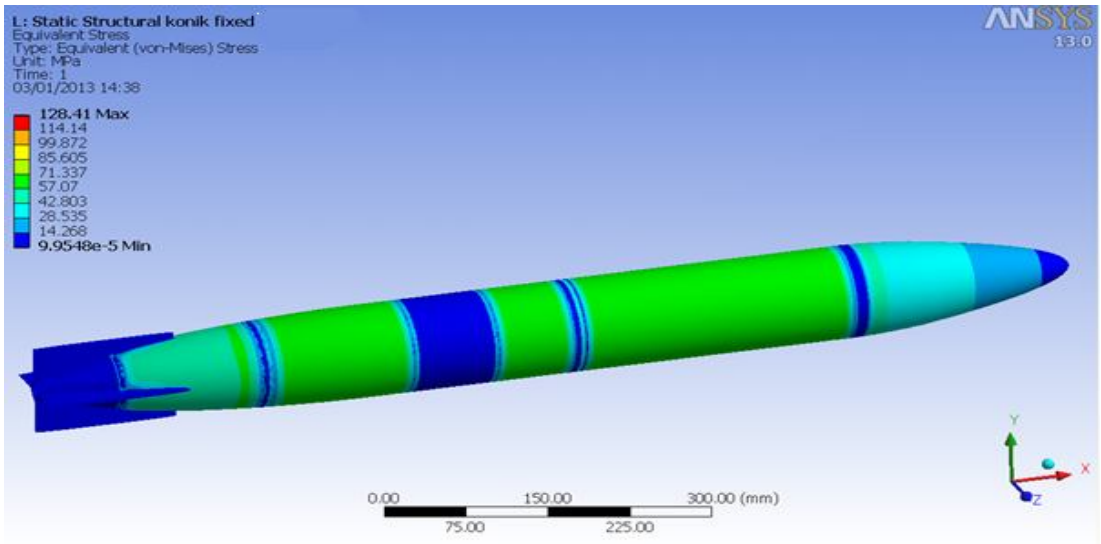

Figure 5.4: Equivalent (von-Mises) Stresses

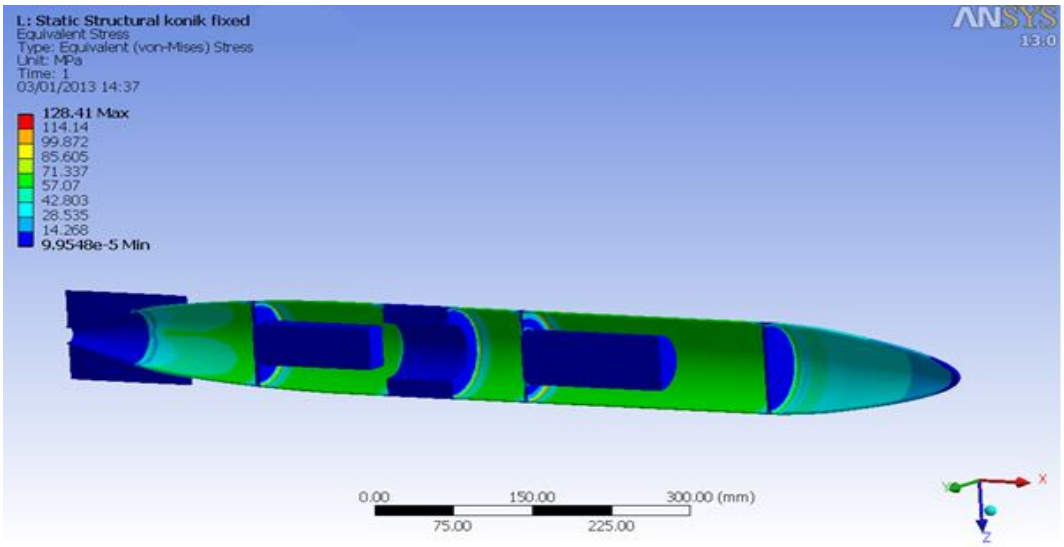

Figure 5.5: Section View of Equivalent (von-Mises) Stresses

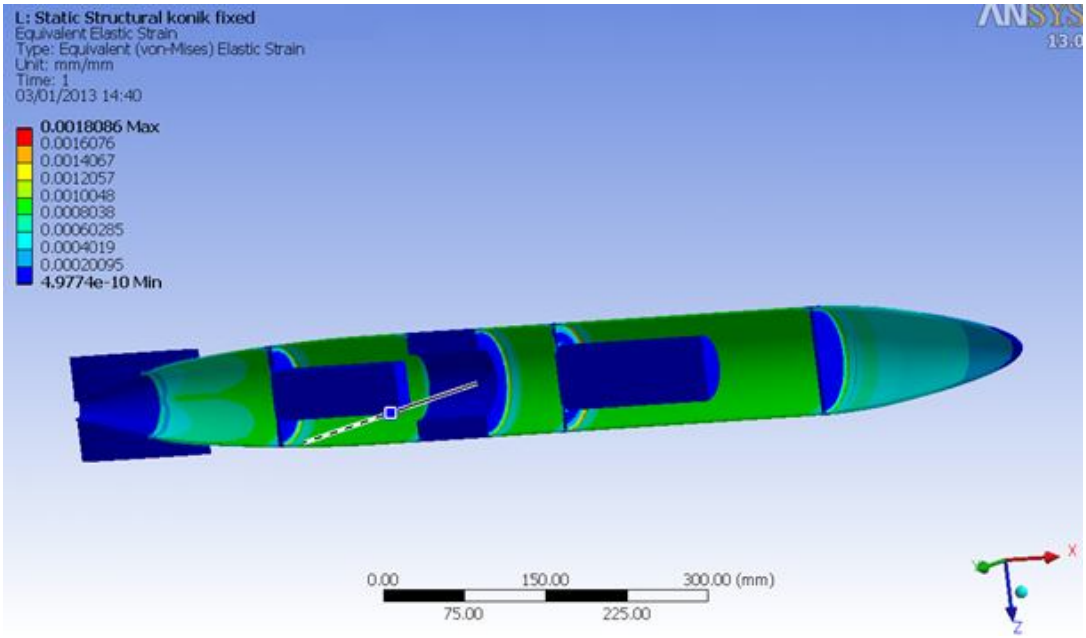

Figure 5.6: Equivalent total deformations

In conclusion, the maximum equivalent stress is about 128 MPa according to Figure 5.4. The equivalent stress is low when we compare the stress with the yield strength of **Confidential** which is 276 MPa. Thus, the target emulator is in safe range.

CHAPTER 6

CONCLUSIONS

In this thesis, an unmanned underwater vehicle is designed and constructed. The vehicle is used as target emulator in defence industry. According to literature surveys, the vehicles are new phenomenon and few applications can be found [Chapter1]

In Chapter 3, the mechanical structure of hull is designed. Firstly, **Confidential** material is selected then the hull thickness is calculated analytically as 2 mm. Thrust system's components are selected and tested. Propeller thrust and roll charts are obtained. The propeller shaft's critical speed is calculated by finite element method. Static and dynamic sealing elements are used to isolate the body from water. The static sealing elements are used between the static hull parts, whereas the dynamic sealing element is used for the rotating propeller shaft. Besides, leakage tests are performed to observe whether the body is watertight. Anti-roll fins and anti-roll weights are used to prevent roll moment created by the propeller. Some stability and speed tests are performed. Adjustable ejector test setup and ropeway test setup are designed to measure stability and speed of the target emulator. Finally, the decoy has been stabilized and has reached about maximum speed of **Confidential**.

In Chapter 4, a control fin mechanism is designed to control decoy. Two alternative control fin systems are designed. They are solenoid control fin system and mini motor control fin system. In addition, two systems are compared in terms of cost, machinability, ease of assembly and etc. In conclusion, the solenoid control fin system is selected and manufactured.

In Chapter 5, finite element analysis is carried out to calculate the stresses on the hull and we compare results of the stress calculations at Chapter 3. An extreme load case is applied to the hull and the load case is simulated. Finally, target emulator body is found to be fairly safe according to the analysis results

In conclusion, when designing the target emulator, we have faced with many mechanical problems. However, problems are solved systematically. The UUV has reached to the maximum speed of **Confidential** without roll movement and has been stable after launching from the ejector. Furthermore, the decoy can be controlled by control fins successfully.

REFERENCES

[1] Rafael Advanced Defense Systems, “Lescut Anti-Torpedo Decoy for Surface Ships”, http://www.rafael.co.il/marketing/SIP_STORAGE/FILES/9/979.pdf, last accessed on 25 /08 /2012

[2] Rafael Advanced Defense Systems, "Scutter Reactive Expendable Acoustic Torpedo Decoy”, http://www.rafael.co.il/marketing/SIP_STORAGE/FILES/9/579.pdf, last accessed on 21 /03 /2012

[3] Whitehead Sistemi Subacquei (WASS), “C310 Anti-Torpedo Countermeasure System for Surface Ships”,http://www.wass.it/WASSWEB/brochure/C310.pdf, last accessed on 18 /02 /2013

[4] Whitehead Sistemi Subacquei (WASS), “C303/S Anti-Torpedo Countermeasure System for Surface Ships”,http://www.wass.it/WASSWEB/brochure/C303.pdf, last accessed on 18 /02 /2013

[5] Ultra Electronics OceanSystems, “Lescut Launched Expendable Scutter”, http://www.ultra-os.com/acoustic.php, last accessed on 03 /04 /2012

[6] Jun, B.H., Park, J. Y., Lee, F.Y., Lee, P.M., Lee, C.M., Kim, K., Lim, Y.K., Oh, J.H., “Development of the AUV ‘ISiMI’ and a free running test in an Ocean Engineering Basin” Ocean Engineering Volume 36, Issue 1, Pages 2-14, January 2009

[7] Jun, B.H., Park, J. Y., Lee, F.Y., Lee, P.M., Lee, C.M., Kim, K., Lim, Y.K., Oh, J.H., “Experiments on vision guided docking of an autonomous underwater vehicle using one camera”, Ocean Engineering Volume 36, Issue 1, Pages 48–61, January 2009

[8] Gonzalez, L.A., “Design, Modelling and Control of an Autonomous Underwater Vehicle”, Bachelor of Engineering Honours Thesis, 2004

[9] “Mechanical properties of Aluminium”, http://ntrs.nasa.gov/archive/nasa/casi.ntrs.nasa.gov/19940033067_1994033067.pdf, last accessed on 28 /03 /2013

[10] Shigley, J.E, Mischke, C.R., “Mechanical Engineering Design”,Vol. 5, pp., 58-60, 1989

[11] Davis J.R., “Corrosion of Aluminum and Aluminum Alloys”, first print, pp., 144-155, 1999

[12] “Coupling”, http://www.princeton.edu/~achaney/tmve/wiki100k/docs/Coupling.html, last accessed on 03 /04 /2012

[13] FAG Technical Product Information, “Single row deep groove ball bearings of Generation C, Schaeffler Group”, http://62.201.97.198/docs/C.pdf, last accessed on 03 /03 /2013

[14] “O-Ring Stocks”, http://www.o-ring-stocks.com/, last accessed on 10/06/2013

[15] Rotary Seals, “Lip Seal”, http://www.roymech.co.uk/Useful_Tables/Seals/Rotary_Seals.html, last accessed on 20/05/2012